Hough Transform application to natural fracture networks: detection, characterization and simulation

Gatien de Callataÿ

Master of Sciences in Applied Earth Sciences
Track Petroleum Engineering and Geosciences

Under the guidance of
Pr. G. Bertotti, Dr. N. Hardebol,
Dr. B. Sirmacek, Ir. K. Bisdom

2015 - 2016

TU Delft

Hough Transform application to natural fracture networks: detection, characterization and simulation

by

Gatien de Callataÿ

to obtain the degree of Master of Science in Applied Earth Sciences
at the Delft University of Technology,
to be defended publicly on Friday October 21, 2016.

Student number: 4381637
Project duration: October 15, 2015 – October 21, 2016
Thesis committee: Giovanni Bertotti, Roderick Lindenbergh,
Nico Hardebol and Kevin Bisdom

This thesis is confidential and cannot be made public until October 21, 2016

TU Delft

Contents

List of Figures

Abstract

UAV imaging is a cutting edge tool for outcrop analysis, in particular because large and/or remote areas can be covered in a matter of minutes. To cope with the large amount of images provided by UAV survey, we have implemented and tested 3 methods to automatically extract fracture patterns: 2 methods based on the colorimetry of the image and one based on the fracture geometry: the Hough transform. These 3 methods lead to mixed results, but the Hough Transform offers an interesting fracture network parametrization. We have shown how this parametrization can be used to describe the spatial distribution of fractures. We later used this parametrization to create a discrete fracture network simulator which takes into account the spatial distribution. Finally, we have compared the performance of this simulator with a random simulator which disregards the spatial distribution. To quantify the performance of the simulators we have tested their well connectivity predictions for various well spacings. These results showed the significance of our approach and encouraged us to further the research to better understand how image analysis techniques could enhance our capabilities to capture fracture network geometry and spatial distribution, and eventually simulate stochastic discrete fracture network.

1 Introduction

Rocks are constituted by mineral aggregates, which form solid matrix and voids which allow fluid transfer. These voids can be pores or fractures (in the following we will use the generic term of fractures to designate any discontinuities in the rock mass such as faults, joints and fractures). Since the 80's, it has been shown that fractures can be the main mode of fluid flow in naturally fractured media [2]. Today, naturally fractured reservoirs make up a large and increasing percentage of the world's hydrocarbon reserves: 60% of world proven oil reserves and 40% of world's gas reserves[1]. Therefore, understanding fluid transfer in these reservoirs has seen a growing interest in order to enhance the hydrocarbon recovery.

The importance of fractures has lead the industry to endeavor to enhance their capabilities to capture and characterize the *in-situ* fracture network's geometrical properties and spatial distribution [30]. Among other techniques, outcrop studies offer hands-on access to fractures, enabling us to perform some measurements not achievable in any other survey, such as the fracture length distribution [3], but also to observe some spatial trends of the fracture network [19].
However, our capabilities to acquire this information are limited to some extent. The location and/or size of some outcrops [7] is an issue since the acquisition and the processing is done manually, limiting the amount of data we can process. Characterizing the spatial trends of fractures and representing it in our predictive fracture model are other common issues [22].

Recent developments in remote sensing technology offer leads to address both the issue of acquiring geologically relevant features such as fractures in outcrops [27] in an accurate and quantitative way and characterizing fracture spatial distribution in a better way [21].

The aim of this thesis is to develop a comprehensive work flow that bridges remote sensing, and in particular image analysis, and fracture network characterization. This work flow integrates automatic fracture network extraction from outcrop images and fracture network simulation based on the opportunities offered by image analysis in the field of fracture network spatial distribution characterization.

In the first part of this thesis we will implement and test automated fracture detection methods based on image analysis techniques and appraise their efficiency. We will also see that beyond extracting the fracture pattern, they offer a new parametrization of the fracture network.
Secondly, we will emphasize how the previously introduced parametrization can successfully capture the spatial distribution of the network and what the limitations are.
In the third and last part, we will highlight how this parametrization can drive a stochastic fracture simulator with enhanced reproduction of the spatial distribution.

This document does not intend to provide a plug-and-play solution to bridge outcrop images analysis and fracture network simulation. However, we want to highlight the potential benefit of an extended

[1] Schlumberger Market Analysis, 2007

multi-disciplinary collaboration between the remote sensing, and in particular image analysis, and geosciences fields of research. This study shows how this would both improve our outcrop interpretation capabilities and our understanding of how much information outcrop images hold with respect to upscale spatial distribution properties.

2

Literature Review

This section intends to provide the reader with some context about the subject of our thesis. We first emphasize how outcrop analyses are made and their limitations. We then review the recent developments in remote sensing and in image analysis. Finally, we will highlight how predictive fracture network models are created, what their limitations are, and how image analysis techniques could offer alternatives.

2.1. Outcrops Study

One of the main focuses of the industry has been to accurately capture the *in-situ* fracture network geometry and its spatial distribution. Indeed, naturally fractured reservoirs may present extremely complex and heterogeneous networks that can have a significant impact on the reservoir production behavior [16].

Well cores and image logs provide valuable in-situ fracture network information on, for example, the fracture spacing, the orientation, the aperture, and cementation. However, some information cannot be acquired through this sampling, such as fracture length [3]; secondly, the fracture sampling strongly depends on well location and inclination; and, finally, the area covered by a borehole is extremely small compared to the reservoir scale [30].
3D seismic surveys cover a much larger area, up to a reservoir scale and beyond, but at a resolution that is typically too low to detect most of the fractures [11].
Therefore, a common complementary method is the characterization of fracture networks from outcropping subsurface analogs. This method offers hands-on access to fractures, enabling us to perform some measurements not achievable in other surveys, such as the length distribution. Outcrops also have the advantage of having a higher resolution than seismic surveys and cover a larger area than borehole images; however, their coverage is still typically below the reservoir scale [11]. In addition to that, outcrops do not provide information about the in-situ fracture network in the subsurface. Therefore, outcrops cannot be used alone to build a reservoir model [26].

Two field techniques are usually used to obtain data from outcropping surfaces. With the first, scan line analysis, we consider the fractures that intersect a set of references lines (scan lines) crossing the rock body. By characterizing each fracture crossing the line, data representative of the formation can be obtained, such as amount of fractures or fracture orientation [12].
The second, outcrop mapping, usually uses geo-referenced photographs on which the fractures can be manually interpreted and traced. Their corresponding attributes such as strike, dip, length and filling can be added. The fractures are then stored as discrete features with their corresponding properties in a database, which is called a Discrete Fracture Network (DFN) [1]. The subsequent analysis of the database aims to establish statistical distributions and relationships between these attributes [30].
However, this methods is fully dependent on the ability of the geologist to accurately interpret large outcrops. Moreover, the amount of images to be interpreted can be extremely large, causing a real feasibility issue [7].

2.2. Remote Sensing Development

Remote sensing technology has improved a great deal in recent decades and the miniaturization of sensors and imagery systems has paved the way for the use of Unmanned Aerial Vehicles (UAVs) for a wide range of remote sensing applications. These improvements have only become possible recently as these systems have become affordable for research and commercial entities, hitherto confined to military [10]. The spatial resolution available from conventional imaging techniques, such as satellites and manned aircraft, is typically in the range of 20–50 cm/pixel, whereas UAVs are able to fly at much lower altitude, therefore with a considerably improved resolution: up to 1cm [27].

Figure 2.1: A UAV with its movable digital camera underneath. The UAV has a diameter of 540 mm and a height of 230 mm. This drone has been used in outcrops images acquisition for most of the outcrops images used in this thesis. *Source: van Eijk* (2014)

Concurrent to the development of acquisition techniques, improvement also has been made with image processing techniques, in particular photogrammetry. Photogrammetry is a technique that captures 3D information of features from two or more photographs of the same object, obtained from different angles [31]. Specifically, structure from Motion (SfM) is a photogrammetry algorithm that creates 3D point clouds from a series of overlapping photos (figure 2.2). SfM allows us to build a surface model and eventually generates orthorectified photomosaics [29]. The orthorectification aims to correct the inclination of the camera, correct the parallax error committed and, finally, the optical distortions of the lens and camera [31].

These high definition surface models, remotely acquired, enable us to overcome many problems caused by direct fieldwork observations. We can cite the difficulty to access the outcrops or their intrinsic hazards (e.g. steep slope or cliffs) [8] as reasons why field observations may be difficult. This acquisition technique is even more useful for horizontal outcrops, where aerial imaging provides the necessary perspective. Furthermore, very large digital datasets can be collected in a matter of minutes. [29].

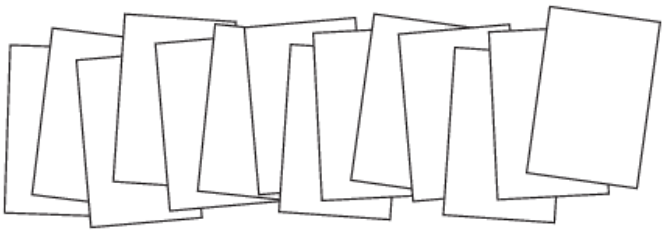

Figure 2.2: Sketch map of overlapping images acquired by a UAV.

2.3. Image Description

An example of outcrop image acquired with a light-weight UAV can be seen in figure 2.3.

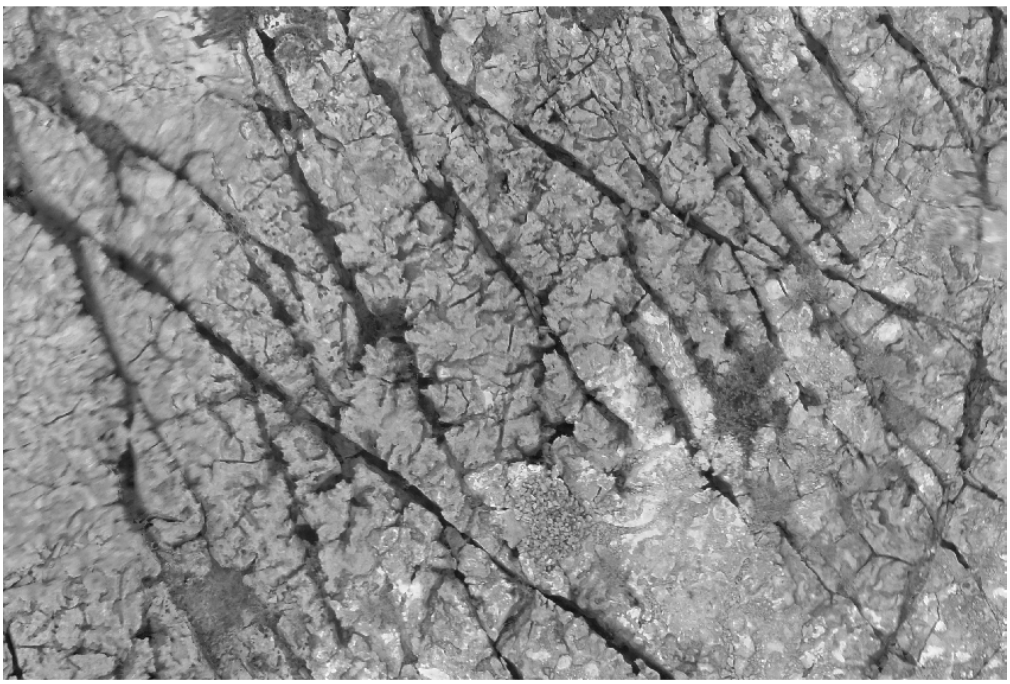

Figure 2.3: Outcrop images acquired with light-weight UAV. *Source: Bisdom 2011*

In the image, fractures can be visually observed due to their furrow-like traces on the terrain. These grooves result in shadows that shade the fractures, which appear as dark-colored features. Other darker features are also present on the image, mainly vegetation. Therefore, fractures are also characterized by their geometry, which is mostly linear.
In the framework of this thesis, we will mainly work on these types of fracture networks due to the visual evidence of fracture traces. It makes the interpretation process easier but, as covered in the next section, also allow us to use iamge analysis based methods.

2.4. Image Analysis

UAV imaging is an edge-cutting tool in terms of acquisition, but, in terms of processing, manual interpretation remains the most commonly used approach. However, manual interpretation is a subjective and time consuming process and is highly dependent on human experience and ability. Therefore, to become a real alternative (both in terms of productivity as well as accuracy) to a traditional survey, aerial imaging needs to be completed with automated processing software tools, necessary to allow the efficient detection of fractures from a large data set of images. Yet, currently no established fully automated method exists [8].

Detecting features in aerial images is a live issue in Remote Sensing research. Some methods intend to address this issue based on the colorimetry of the image. An example is road detection from aerial images. Based on the observation that roads have similar pixel colors on the images, they can be detected by detecting color invariant features [24]. A medical investigation also addressed the issue of detecting fractures in bones using image colorimetry [17]. In his work, *Mahendran* (2012) shows the possibility of automatically detecting fractures in X-Ray images by finding sharp variations in color in the image, indicating bone discontinuity, using various edge detectors.
These applications are transposable in the field of geological fracture detection.

Instead of using the colorimetry, *Vasuki et al.* (2014) introduced a semi-automated method based on the hypothesis that fractures are lineaments, using the Hough Transform to extract linear fractures on 2D binary images. The Hough transform is a mathematical method which intends to identify colinear points in a binary image. This is done through a voting procedure carried out in the parameteric space used to describe lineaments: each point votes for all lines possibly going through them. Lineaments are then the local maxima in the parametric space[1].
In this method the Hough transform is used to propose to the user an exhaustive set of lines, potentially fractures, among which they can select the ones that are geologically significant and then eventually merge the traces that belong to the same fracture.
This method achieves promising results with a bit less than 80% of the fractures correctly detected when compared to a manual interpretation. The time efficiency is also demonstrated with only 10 minutes of processing compared to 7h of manual tracking. This method is cutting-edge since it uses a relatively new tool, the Hough Transform, to parametrize fractures. However, this method is limited due to the need of a user for post processing, and also due to detection rates that are still too low.

The need to rely on a semi-automated Hough method can be explained by the limitation of the Hough Transform highlighted by *Karnieli et al.* (1996). In this study hightlights the difficulties the Hough Approach has in dealing with multi-scale fracture networks, and the tendency of detecting only major lineaments. To deal with this issue, *Vasuki et al.* (2014) introduced some parameters that can be tuned in the Hough space analysis to allow the detection of fractures of different scales. But, this tuning is done manually, leaving an important gap between its current state and the full automation of Hough-based fracture detection tools.

If the possibilities of automation of the Hough Transform method to detect fractures in outcrop images are still limited to semi automated methods, some show the possibility to characterize the spatial distribution of existing data sets using the Hough parametrization [23].

In their work, *Pochet et al.* (2013) show the possibility to drive a discrete fracture network simulator based on the Hough transform, and in particular how to deduce orientation and position of fracture planes from Hough space analysis. Based on micro seismic event occurring during hydraulic fracturation, one may transpose each of these event in the Hough space. A subsequent analysis of the Hough space may reveal some spatial trends of the fractures. However this description is applied only to a cloud of points, and not to the entire network. Therefore this description obtained in the Hough space doesn't intend to fully characterize the entirety of the network but only the fractures that play a role during the hydraulic fracturation.

[1] More will be covered about Hough transform in chapter 3.

2.5. Discrete Fracture Network Simulation

Outcrops, and even more so boreholes, are usually small compared to the reservoir size [11]. Thus we need to extend our partial knowledge of the reservoir. To do so, we can construct a statistical discrete fracture model spanning over the entire reservoir. This model takes, as input, the fracture properties' statistical distribution observed in borehole logs, seismic surveys, and outcrops studies [3][22], and integrates these distributions through space [2][13]. The position of the fractures is then stochastically determined with a heterogeneous *Poisson Point Process* [25] following a fracture density map. Many studies have shown the possibility to generate a reservoir scale fracture model based on the spatial integration of these statistical distributions derived from field and outcrops measurements [15].

Nevertheless, there is no guarantee about the quality of the model, and, in particular, some spatial trends observed in the field, such as the spacing of the fractures, are not trivial to reproduce in a stochastic simulator. Failing to capture the spatial trends of the network may impair the quality of the model, and eventually result in poor reservoir predictions.

Here we propose an example to illustrate the importance of capturing the spatial distribution of the fracture network. In figure 2.4, we compare a natural fracture network, observed in an 18x18m sandstone outcrop in Norway, and a stochastic realization of randomly located straight-lines which are similar to the natural pattern in all respects, including length and orientation distribution, but not the spatial distribution. The fractures have been implanted using the *Poisson Point Process*

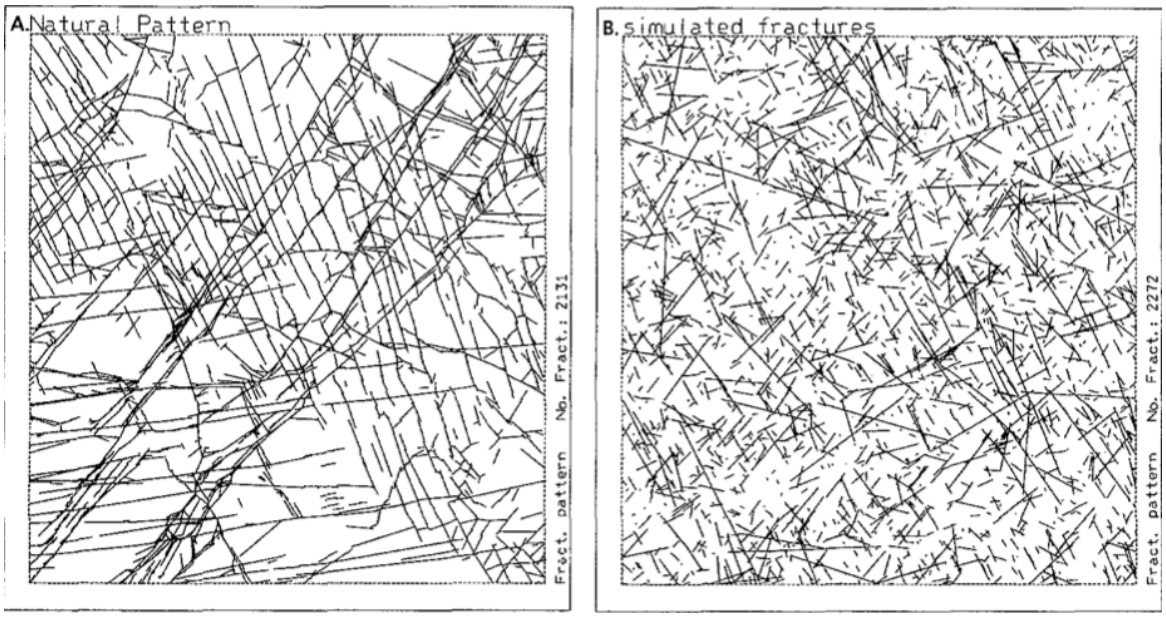

Figure 2.4: (a) The natural pattern mapped from an 18 x 18 m area on the surface of a sandstone layer from western Norway. (b) An example of the realizations of randomly spatially distributed line segments which have similar orientations and length distributions and line segment density to the natural pattern. *Source: Odling* (1992).

The difference between the natural network and the random realization is visually perceptible, despite having similar orientations and length distributions and fracture density. This is because in figure 2.4(a) neighboring fractures show similar orientations, and tend to be coaxial, giving the impression, on one hand, of longer fractures in case (a) and, on the other hand, of parallelism, which is not apparent in case (b).
We can also highlight the difference of topology. The topology essentially describes the relationship between fractures in a network and, in particular, the way they intersect and terminate. In the natural network, there is a significant amount of type T connections (i.e. fracture tip terminating on the trace of another), which are a rarity in the random model where almost all the intersections are of type X (i.e. fracture traces crossing each other), or type I (i.e. loose ending fractures).

In terms of the matrix properties and, in particular, the connectivity, these two networks strongly differ. The condition for two fractures being connected is if there is a cluster (a set of fractures that are connected [2], where connectivity refers, in this thesis, to the instances where fractures intersect one another) containing both of them.
Therefore, the main attributes that control connectivity are the clustering, and, in particular, the size of the largest cluster [19].
In the natural case, clusters tend to be larger. In particular, the largest clusters represent 70% of the total network trace length, while, in the random realization, they only represent 25% [19]. Therefore higher connectivity can be expected in the natural network.
Such stochastic modeling will fail to capture the structure of the network and, hence, may fail to model the underlying transport properties of the system [22], which may, in turn, result in unrealistic predictions of either fluid flow or production behavior [20]. *Odling* (1992) shows in her work that random realizations underestimate the probability of connectivity between two wells spaced by 18 m by a factor of 10.

The specific spatial arrangement of the natural network is not trivial to reproduce in a stochastic way. Different ways exist endeavoring to reproduce the spatial structure of the network. *Odling* (1992) proposes to tackle this issue by using an approach based on the P21 (i.e. the fracture intensity: the total trace length per unit area). In this method the outcrop is divided into multiple boxes and their average P21 is computed. Then we create a new box of a similar size where we successively add fractures to it. After each line segment is added, the P21 within the box is calculated and generation is stopped when the density reaches the average P21 of the natural pattern. We then repeat this process until the number of boxes we created covers the desired area.

Another way to keep the network structure is to use the topology. In *Sanderson and Nixon* (2015) a stochastic simulation honoring the proportion of each type of fracture termination and intersection tends to improve the rendering of some network characteristics such as connectivity.

In this thesis, we will try an alternate method, the Hough transform, as a way to connect the dots between Remote Sensing, and in particular image analysis, and fracture network analysis and, ultimately, simulation.

3

Image Analysis for Fracture Trace Extraction

The aim of this section is to evaluate how automatic methods can be used to help geologists extract relevant fracture network information from outcrop images. After presenting the type of images used in this thesis, we are going to test a number of automated tracing methods to see if they can be used to extract fracture data. The implementation and testing of these techniques will be performed with MATLAB. We will focus on the tracing itself but we will also see that they can offer a means to capture the spatial distribution of the network.

Beforehand we will introduce two metrics to quantify the accuracy of the automated detection:

- False positive ratio is the proportion of detected features in the automated method that are not fractures according a manual interpretation. The ratio is calculated as $F = \frac{L_w}{L_d}$, where L_w is the total trace length of detected features that are not actual fractures and L_d is the total trace length of detected features.
- Recall ratio is the proportion of the manually interpreted fracture network that have been correctly detected. The ratio is calculated as $R = \frac{L_c}{L_t}$, where L_c is the total length of the faults identified by the automated method and and L_t is the total length of faults identified in manual interpretation. The amount of undetected fractures is then: $(1 - R)L_t$.

3.1. Straightforward Fractures Tracing Method

Straight forward methods aim to trace fracture networks exclusively based on the colorimetry of the image. In this approach we detect fractures using basic image processing and computer vision algorithms. They are called straightforward because they are fast and easy to implement, but they disregard any geological input such as expected fracture density or length/orientation distribution that may determine if the detected features are really fractures. We have tested two of these methods: the Snake Method and the Advanced Skeleton (AS).

3.1.1. The snake method

The snake method derives from a remote sensing application to detect road networks on aerial images by detecting color invariant features as described in the literature review [24]. In some ways fracture networks can be similar to road networks, in particular in terms of geometry (i.e. a network of linear features) and color invariance, therefore similar methods can be applied.

We have implemented a function to detect such invariant features based on the gray level gradient of the grayscale image. The function, when given a seed point in a fracture, starts to propagate following the path where the gray level remains the most constant, therefore within our color invariant feature. Like a snake crawling in the fracture pattern, it will jump from a pixel toward the next in the direction

where it detects the flattest gray level gradient. Eventually, the path followed by the ”snake” is the fracture pattern.

The function detects the flattest gradient using a finite difference method (FDM). The precision of the FDM is called the radius of investigation. The user can set this radius, *d*, within which the snake will detect the flattest slope. Hence the FDM formula is given by:

$$min(\frac{1}{d}\sum_{i=1}^{d}|p_0 - p_i|;\ \text{for each direction}) \tag{3.1}$$

3.2.1.1 Results

We've tested our function on two images. First, a satellite image of a river, which is similar to a fracture in the sense that we observe a clear contrast between the object (river) and the surroundings. Our detection performed accurately but has been limited in the final result due to its inability to follow multiple traces if we reach a branch point (figure 3.1).
Secondly, we tested the method on an outcrop image (figure 3.2(a)). This test has highlighted that the snake function may be extremely unstable. This is characterized by the fact that if the snake gets out of the trace it will propagate permanently outside since it will follow a gray level which is not representative of the fracture anymore.

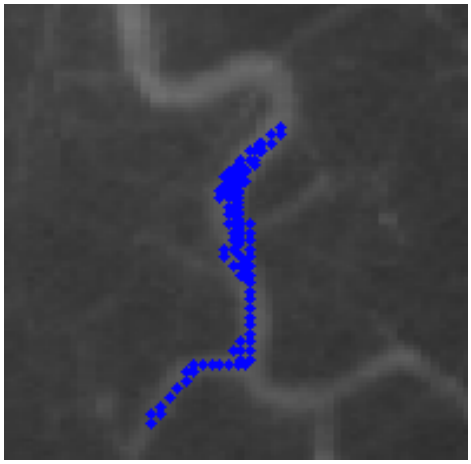

Figure 3.1: Detected trace with the snake function, used on a satellite image of a river

The snake goes out of the trace when the gray level gradient within the fracture trace is steeper than the edge gradient. This situation is observed if the gradient within the fracture is sharp, such as, for example, fracture discontinuity or vegetation inside the fracture, or if the gray level gradient of the edge is smooth, such as, for example, if the image is locally blurred. This can be seen in figure 3.2, after iteration 60, due to blurring, the snake chooses a wrong direction. This is irreversible, and the snake follows a gray level, corresponding to the surroundings, permanently as seen in figure 3.2(b).

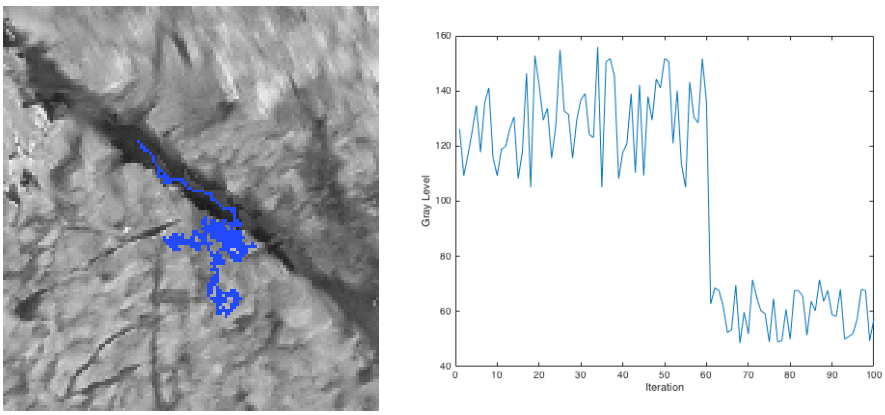

Figure 3.2: (a) Detected trace with the snake function, used on a aerial image of an outcrop. (b) Gray level followed after each iteration.

A way to deal with this recurrent issue would be to stop the tracking when we observe a large variation in the gray level, as observed in figure 3.2(b). Then, request the user to provide a new seed. However,

that would definitely impair the ability of the snake to be autonomous, which is the purpose we endeavor to achieve.

These considerations show that the snake can be very powerful if the conditions are suitable, as in the figure 3.1, with sharp fractures edges, continuous traces and no blurring. But, since it cannot deal concurrently with multiple traces and is unable to deal with fracture discontinuity and local blurring, the application of this method to an outcrop image is therefore limited to some specific cases that meet all these criteria.

3.1.2. The Advanced Skeleton

3.2.2.1 Methodology

Observations of an outcrop picture show us that fractures are usually the darker elements, due to the shadow induced by the relief. Therefore, if we threshold the picture to the highest gray-level, we could extract a rough network shape. The Advanced Skeleton (AS) is a way to refine this imperfect shape and eventually provide a fracture network represented by a collection of lines.

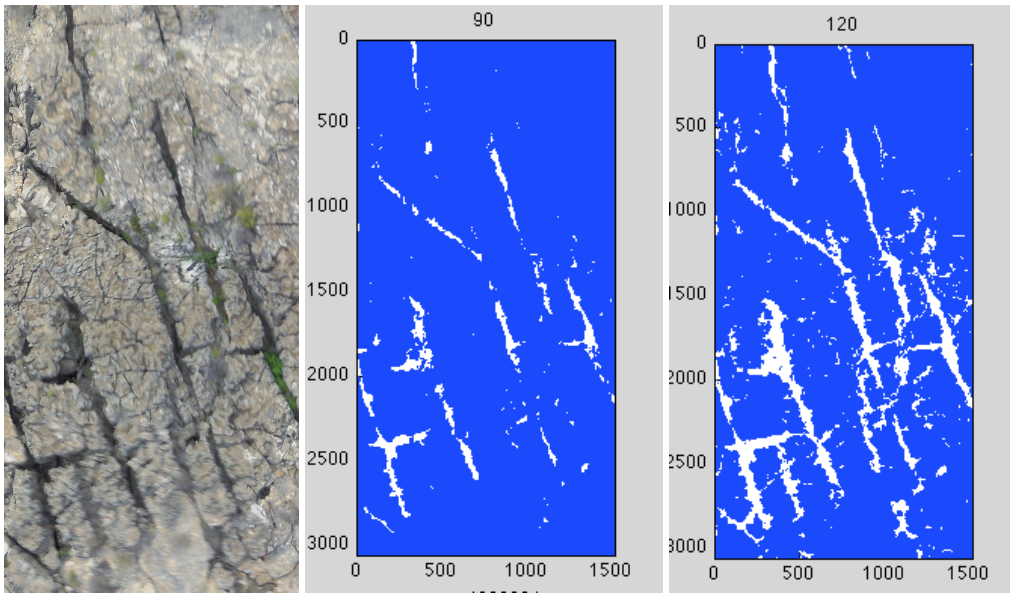

Figure 3.3: Thresholding at different gray level, from left to right: original picture, threshold at 90, and 120

We can see on figure 3.3, for increasing threshold values, the depiction of the fracture network increases, more fractures are detected and they look more continuous. But, increasing the threshold also leads to a noisier image. We observe here three types of noise: salt-and-pepper noise (i.e. detected features of the size of only few pixels [9]), external noise (i.e. features that are not fractures such as vegetation) and dissolution noise (i.e. complex and tortuous fracture edges).
In particular, salt-and-pepper and external noise tend to increase with a higher threshold. This correlation can be explained by the fact that as the threshold increases, more external features, such as trees, are captured resulting in external noise; as are some small local background elements, resulting in salt-and-pepper noise.

Dissolution noise appears when the edge of the fractures are vague, either due to natural weathering or because the image is locally blurred. These unclear margins tend to be detected alongside their respective fractures. Therefore this noise is present at every threshold level.
Therefore, a good balance needs to be reached between an exhaustive detection which is noise prone, or a limited detection with little noise.

We introduced the AS method to allow a high threshold while eliminating the salt-and-pepper and dissolution noise. First, we perform a morphological filtering operation to remove salt-and-pepper noise.

This is achieved by removing every features of a size under a certain threshold [9]. The threshold is easy to select since there is a difference in magnitude by a factor 100 between salt-and-pepper noise and actual fractures.

Then we use the a skeleton operator to trim the noise dissolution and reduce the binary image to a bundle of strings, which are representative of the fractures. The skeleton operator is a an algorithm that continuously removes pixels on the boundaries of objects but will not allows objects to break apart [9]. The pixels remaining make up the image skeleton, as seen in figure 3.4.

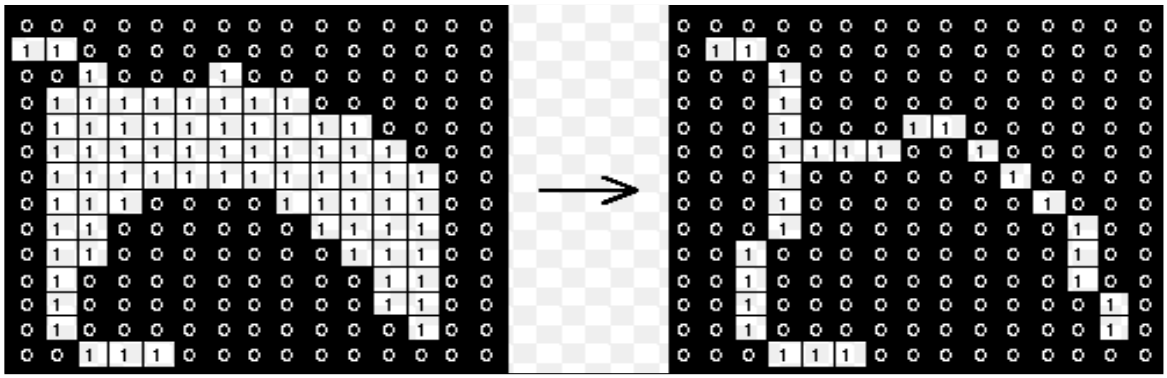

Figure 3.4: Conceptual description of the Skeleton Operator on a binary image. *Credit: Apache Technology Ltd.*

In this process, many unwanted skeleton branches are created, triggered by the uneven edges of fractures on the binary image (the dissolution noise). This effect can be seen in figure 3.4: we have a semicircular feature with uneven edges: for instance, we observe a little spur on the top-left. This spur will lead to the creation of a branch that is not representative of the feature.
Removing unwanted branches is a difficult step since we don't have a universal criterion to determine if a branch is relevant or not. What we can do however, since most of the branches are triggered by spurs, is to remove all the terminating branches (between an endpoint of the skeleton and the next branch connection), and repeat this operation. We then make the assumption that most of the branches are artifacts.

3.2.2.2 Results

In the figure 3.5, we see the result of the application of the skeleton and the Advanced Skeleton after 2 subsequent branch removals. In particular, we can observe the difference between the two. The results are encouraging, since a comprehensive detection have been performed with a very limited amount of noise. The recall rate is very high compared with the model performed manually by a trained geologist, which tends to confirm that our assumption of most of the branches being artifacts is correct.

Yet, this model has a flaw, as seen in the red box in figure 3.5: a previously continuous trace has been divided in two distinct segments by the branch removal. The output we generate with the AS method is therefore questionable since some fractures may have been altered. In addition to that, the output of the AS method is not really neat in the sense that there are still unwanted branches and detected fracture are tortuous (where traditional interpretation usually favors straight lines). Furthermore, external noise, such as vegetation, remains despite the branch removal.

To address these issues and enhance our AS method, we propose a method in the next section which can take into account some geological input (unlike straightforward methods), such as the shape of the fracture (lineament), the minimum length of the fractures or the possible orientations.

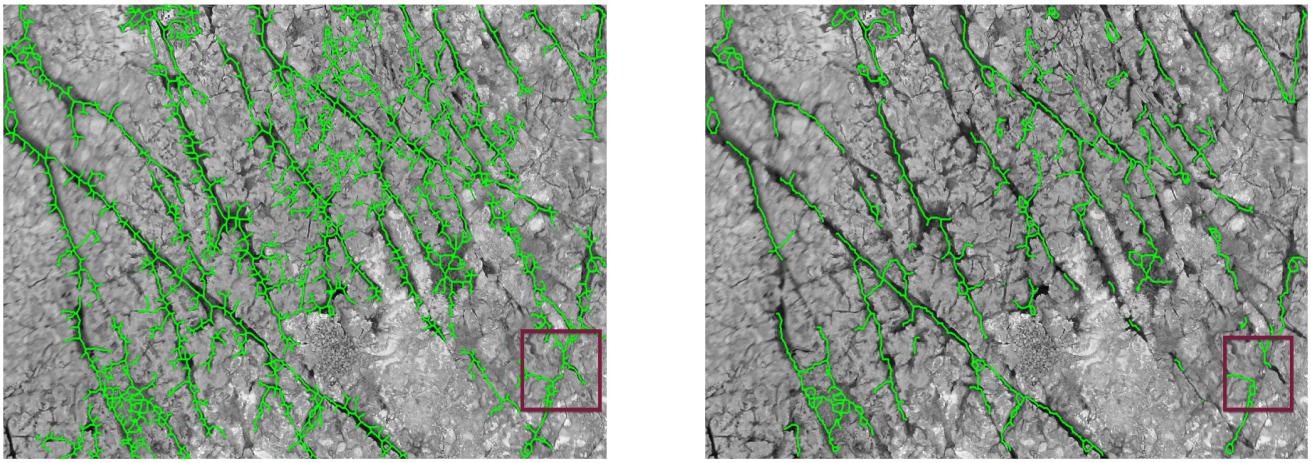

Figure 3.5: (a) The initial skeleton. (b) Advanced skeleton (after 2 successive branch removal operation).

3.2. The Hough Transform Method

As covered in the literature review, the Hough Transform Method (HTM) offers an way to extract linear features in a binary image. Fractures can be considered to some extent as linear, therefore this method would offer an innovative way to identify fractures on outcrop images.
This method can also account for geological input because we can limit the detection to certain shapes (lines) and certain parameters (i.e. orientation distribution, fracture density, minimum fracture trace length...).

3.2.1. The Hough transformation

The equation of a line can be expressed in a parametric form as: $\rho = xcos(\theta) + ysin(\theta)$, where ρ is the distance to an arbitrary origin of the closest point on the axis of the line, and θ the angle between the x-axis and the line connecting the origin to that closest point (figure 3.6) [6].

The Hough transform will take advantage of this parametrization to detect the presence of lines described by $\rho = xcos(\theta) + ysin(\theta)$.
Given a point (x,y) on the image, we can identify all the parameters (ρ,θ) that "agree" with that point as those that correspond to all the lines that pass through (x,y). Each image point (x,y) will thus correspond to a sinusoidal trace in the Hough space (figure 3.7.

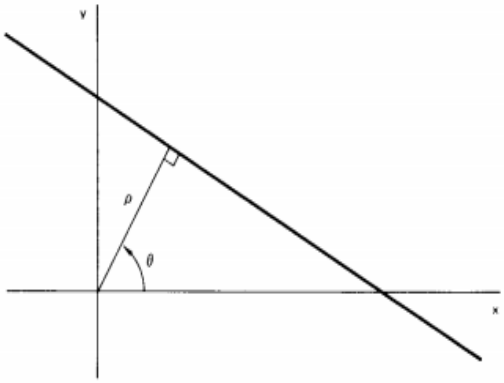

Figure 3.6: paramteric equation of a line *Source: Dud and Hart* (1972)

This method is implemented in MATLAB[1]: a 2 dimensional matrix, also called a Hough Matrix or accumulator array, where each bin corresponds to a pair of $< \rho,\theta >$, is created. Then, for each non-null pixel in a binary image, we will calculate all the possible pairs of $< \rho,\theta >$, corresponding to all the possible lines going through it, and increment the corresponding bin in the accumulator [6]. Therefore colinear points will vote multiple times for the same bin, highlighting the presence of a lineament.

[1] In MATLAB θ, is defined by the angle of the lineament itself with the y-axis, clockwise [18]

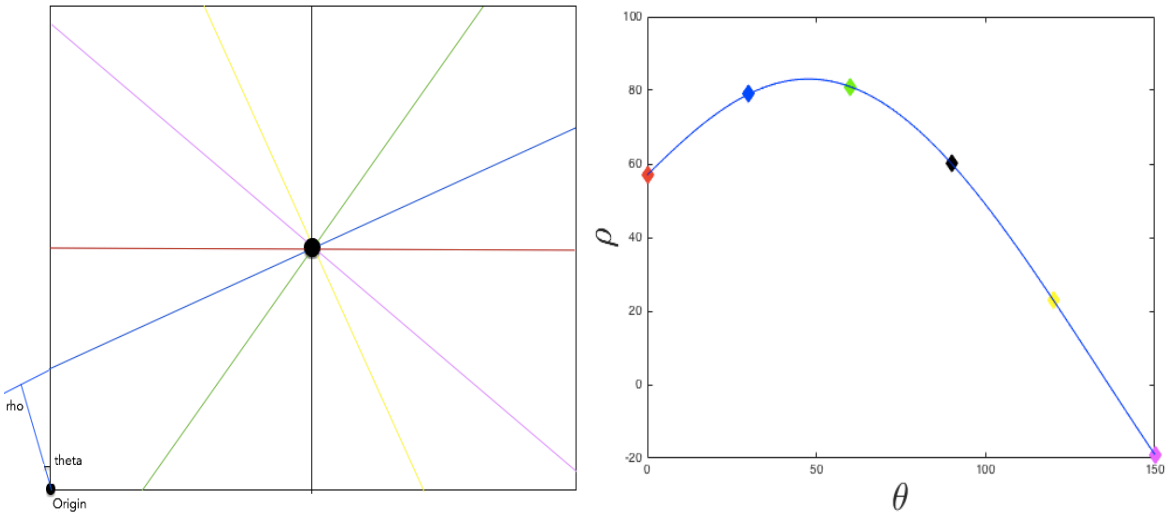

Figure 3.7: Sinusoidal trace of a point in the Hough space.

As an example, in figure 3.8, 3 pixels are aligned on an axis characterized by $< \rho = 10, \theta = 1rad >$. We see their respective sinusoidal traces in the Hough space in figure (b). Each trace (point) will increment once for each bin that it crosses. This voting approach shows evidence of lines for each peak present in the accumulator. The longer the lineament is, the higher peak.
Obviously if a pixel has a slight offset to the axis, for example in the case of a curvy trace, it will not increment the correct bin. Therefore it will lead to a so-called peak's dilution, where the value of the peak is below the real amount of pixels present in the trace.

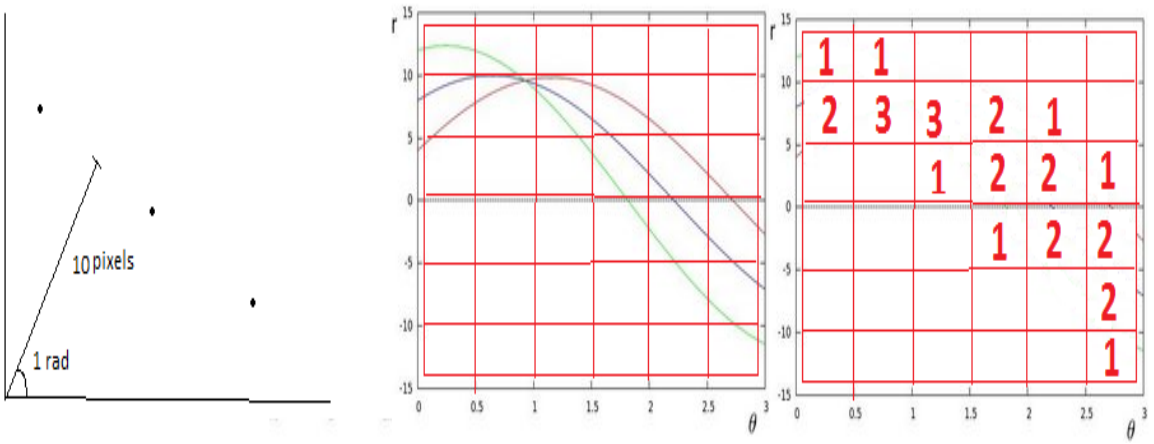

Figure 3.8: (a) 3 colinear points. (b) In the Hough domain: each sinusoidal trace is the transform of 1 point. (c) Each bin value is the the number of traces (points) going through this bin. A peak (value=3) is seen at the coordinate of the colinear axis.

3.2.2. Methodology

Identifying lineaments, and thus fractures, on the outcrop images can be achieved in two steps: first transforming the image into a binary image that keeps only fracture-like elements, then transforming the binary image into the Hough space and extracting the lineaments from the Hough diagram.

This method already has been implemented on a semi-automated basis. In their work, *Vasuki et al.* (2014) binarize the image using an edge detector, then they transform it into the Hough space. Then, the peaks are detected in the Hough space. However, the peak extraction cannot be done straightforwardly, non fractures element on the binary image can either create unwanted peaks or mask accurate ones. To overcome this issue, *Vasuki et al.* (2014) introduces 4 criteria as a way to discriminate whether peaks correspond to a fracture trace or not. These criteria will be: the range of possible orientations, the minimal lineament length, the maximal discontinuity within a lineament and the minimal spacing between two lineaments. The criteria values are selected empirically on one specific image, and the user is ultimately responsible to refine the output by removing false positives and adding traces left undetected by the method [29].

We propose here an alternative method which is fully automated. In a first stage, we propose to study how we can enhance the binarization using our previously introduced Advanced Skeleton.
Then we will study the influence and sensitivity of the 4 criteria. We want to understand how different criterion values influence the efficiency of the Hough method to ultimately develop an automated selection strategy that could adapt to many different images or fracture networks. Indeed, an empirical selection of the criteria with a large data set is not possible since images, but also fractures, may be extremely different.
Eventually, based on our result we will introduce an automation of the Hough Transform Method.

3.2.3. Binarization and Criterion Study

Binarization of the image

To obtain the binary image, input for the Hough transform, *Vasuki et al.* (2014) suggest to use a Canny edge detector. This detector will find sharp gradients in the gray level and extract them as the boundaries of elements (figure 3.9). This approach is not suitable in our case for two main reasons.
First, fractures may not be the only features present on the image. Unevenness of the rock, vegetation, power lines and roads will provide many unwanted edges.
The second reason is due to the vagueness of the edges. Therefore, the edges of fractures will be either not detected or they will be very irregular. This will later lead to the softening of the peaks in the Hough Transform, since peaks are enhanced by the amount of aligned pixels.

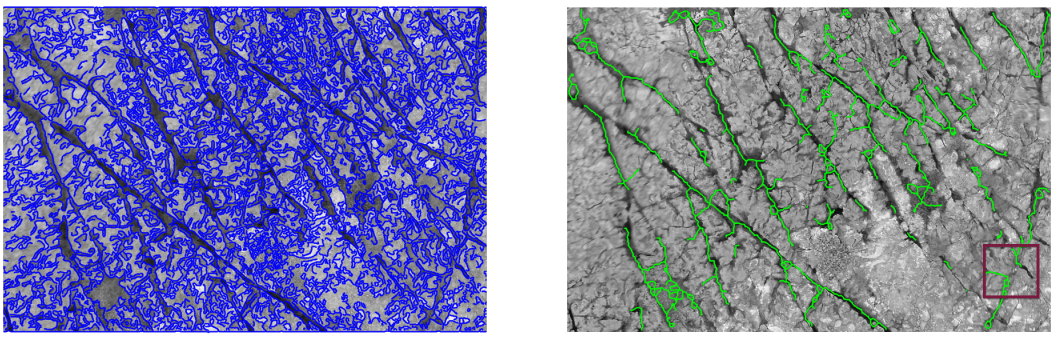

Figure 3.9: Comparison of two binarization techniques: (a) Canny Edge Detector (b) AS method (b).

Therefore, we decided to binarize the image using the AS method. The AS approach has proven its ability to deal with dissolution noise and provides a binary image that is already representative of the fracture network.

The domain of the Hough Transform

With regular patterns, in which all the fractures follow one or two main directions, we can define the boundaries of the Hough Domain to certain angles. By limiting the admissible lines to a certain range of angles, many false positives will be removed without further processing.
In the example 3.10, bounding the domain avoids many false positives. However with more complex

patterns, where the range of fracture orientations is very wide, this concept become obsolete.

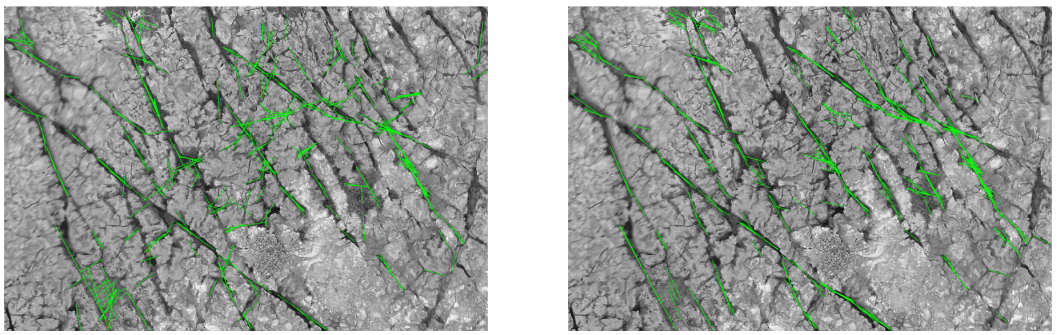

Figure 3.10: Comparison between an unbounded Hough Domain (LEFT) and a Domain limited to angle range of -80° to -20° (RIGHT).

Minimum Length

This criterion defines the minimal length of detected features. Below this minimum, object are disregarded.

In the figure 3.11, reducing the minimal length triggers the detection of many small scale artifacts; however, it also increases the detection of real fractures, which are often a collection of small lineament segments.

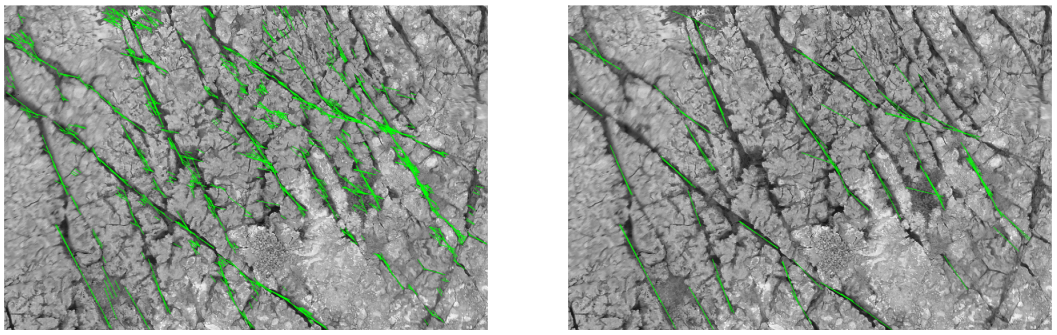

Figure 3.11: Comparison between a minimum length of 10 pixels (LEFT) and 60 pixels (RIGHT).

Maximum Lineament Discontinuity

To overcome the previously mentioned discontinuity issue, we can also decide that below a certain gap, lines that are on the same axis should be merged.

It is difficult to asses weather two traces on the same axis are really members of a unique fracture. In the figure 3.12 many small features on the axis -10° are erroneously merged. However continuity of real fractures is more respected. Only a thorough geological assessment, which the computer is unable to do, can it be determined which merged lineaments are relevant or not.

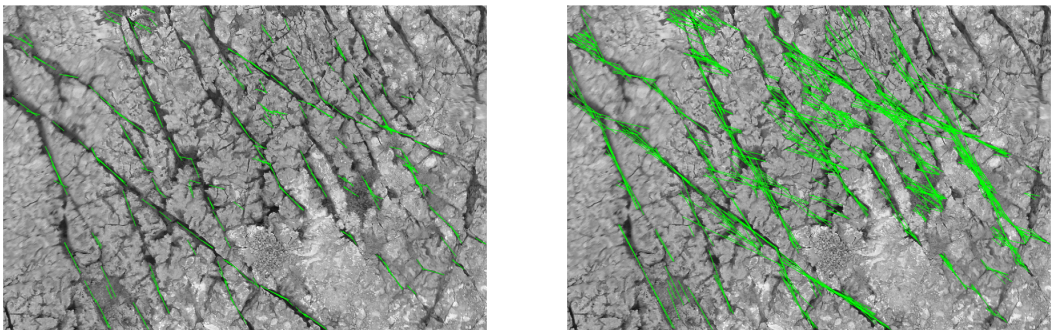

Figure 3.12: Comparison between maximum gap of 10 pixels (LEFT) and 30 pixels (RIGHT).

The Cancellation Range

When we extract the peaks, we set the accumulator in a certain range around the peak to zero, in what we call the cancellation zone. This aims to avoid picking up two peaks that are very close and may represent the same feature. Extending the cancellation zone may remove multiples (i. e. detected features representing the same fracture, figure 3.13), but may also cancel other distinct fracture close to each others.

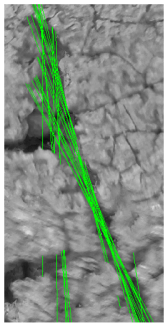

Figure 3.13: An example of multiple in HTM

Discussion

As exemplified in the above figures, variation in the criterion values generates different results. The results differ in their precision, their accuracy and their resolution, yet no optimum is easily reachable. We always either favor a conservative approach with a low recall rate but a very low rate of false positives, or the opposite, an optimistic approach with a high false positive rate, but a high recall rate. This can seen in table 3.1.

Figure	Recall ratio	False positive ratio
3.10(a)	High	High
3.10(b)	Moderate	Low
3.11(a)	High	Moderate
3.11(b)	Very Low	Very Low
3.12(a)	Moderate	Low
3.12(b)	High	High

Quality Scale
Good
Moderate
Poor
Very poor

Table 3.1: Qualitative recall and false positive ratios for the above figures. There are no cases of a good recall and false positive ratio.

These results tend to indicate a high variability in outputs, and show that an optimal deterministic set of criteria does not necessarily exist. By optimum we mean a set of values that trigger a comprehensive network detection -high recall ratio- with a low amount of noise -false positive ratio-.

However, we also need to weigh these different results from a geological perspective. Indeed, some results, despite having lower recall ratios, increase the geological significance. For instance, the minimal length criterion is relevant when we study multi-scale fracture networks, where we are interested in only one given size scale. Withal, the maximum lineament discontinuity criterion allow us to accurately detect large fractures despite the fact that they appear discontinuous in the outcrop. Finally, the definition of the Hough domain allows us to focus on only one given fracture orientation set.

3.2.4. Hough Transform using Monte Carlo Simulation

To overcome the difficulty of finding a deterministic set of optimal criteria values, a stochastic approach, using Monte-Carlo method, has been implemented. In this approach we run the detection method multiple times, applying different criteria values within a predefined range for each realization. Each realization is in the form of a binary image where fractures are 1 while background is 0. Then we superimpose the multiple realizations by adding the different binary images. This intends to create a fracture presence probability map where real fractures, often detected, are discriminated from false fractures, seldom detected, on the basis of the summed up pixel values.

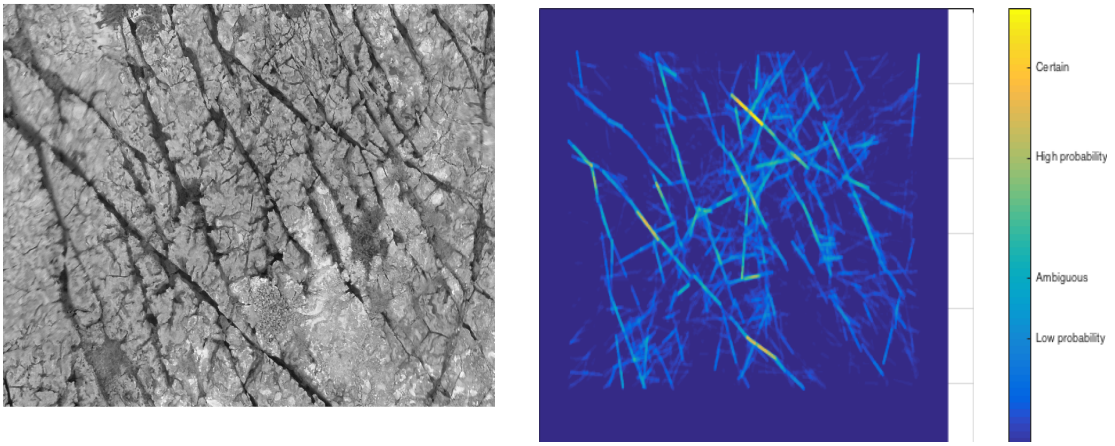

Figure 3.14: Results of the Monte Carlo Simulation with 1000 Runs

The figure, 3.14, represents a Monte-Carlo simulation with 1000 realizations applied to the same outcrop image as in section 3.3. We can see in this probability map that some clear fracture trend appears. This can be seen in figure 3.15, when we compare the features that have been detected 100, 150 and 200 times or more.

These results are encouraging because they show the possibility of achieving extensive detection of the network fully automatically. However, we observe that the extracted network is still impaired by false positive detection and by the discontinuity issue. In particular, for the features detected 200 times or more, there are no fracture traces which remain continuous.

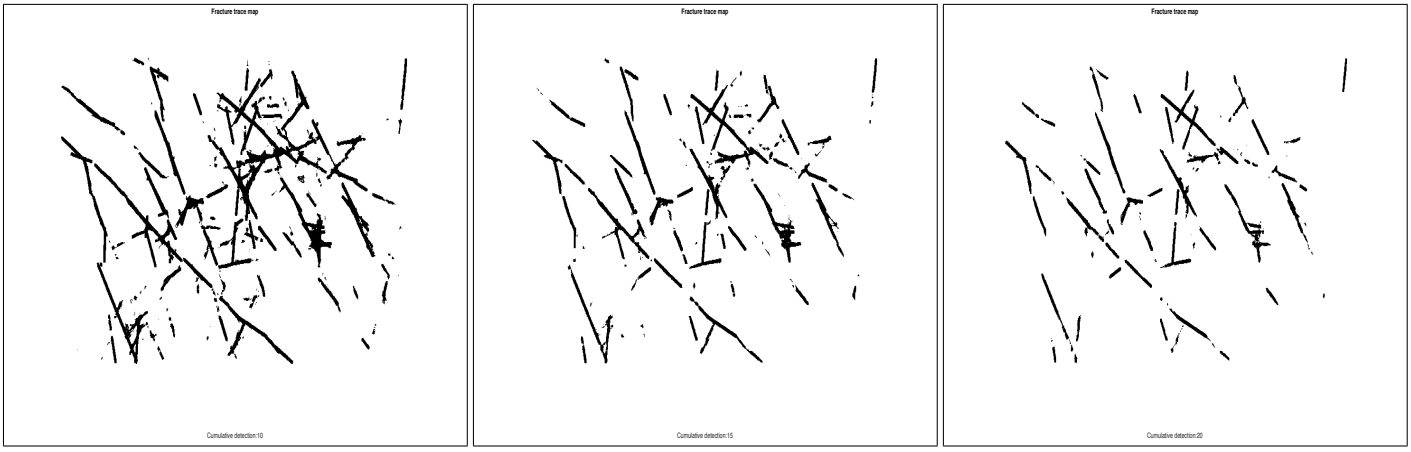

Figure 3.15: Features detected (a) 100 times or more, (b) 150 times or more, (c) 200 times or more.

3.3. Discussion

In this chapter we've been investigating the possibility of having an automated method for fracture tracing. The three different approaches proposed offer promising paths of research. We can compare our three approaches with the following table.

Figure	Recall ratio	False positive ratio	Geological input
Snake Function	-	-	No
Advanced Skeleton	Very High	Moderate	No
Hough Transform (best achieved)	High	Moderate	Yes
Hough Transform (Monte-Carlo)	Variable	Variable	Yes

Table 3.2: Recall and False positive ratio for the Snake, Advanced Skeleton and Hough Transform method.

The snake function hasn't been tested since it has shown too much instability to be properly used with our data set. However, as described earlier, in appropriate situations it may lead to better results.
The Advanced Skeleton is the function that offers the most reliable result, with a very high recall ratio. However, a moderate false positive ratio, induced by the external noise, the tortuosity of detected features, and, finally, the discontinuity issue raised by branch removal make it difficult to use as a reliable model capable of replacing manual fracture tracing done by a trained geologist.

The Hough approach shows some encouraging results, in particular when used in a Monte-Carlo simulation. In particular, from a geological perspective, this approach is an absolute improvement, compared to the previous methods, in the sense that we can limit our detection to some features of interest either in terms of shape (straight lines), size or orientation, which is a missing consideration in the straightforward methods.

Finally, the Hough transform offers an innovative parametrization of the network. The transformation combines the trace length, the orientation and the spatial distribution in the same space, allowing a cross correlation between a fracture's length-orientation-position.
Despite not having extracted the network itself, we may have extracted valuable information to characterize it. In the following sections we will discuss the accuracy and significance of the Hough-based fracture network characterization.

4

Using Hough Transform for Network Characterization

In the previous chapter we've introduced how an image analysis based method, the Hough transform, could offer a new paramterization to characterize fracture networks. In this chapter we will emphasize how this technique can extend our capabilities to capture the spatial distribution and geometry of a fracture network. In the following we define spatial distribution as the way fractures are positioned, underlying that their respective position is not random. This improved characterization is the second bridge in our work flow between image analysis and geology.

In the framework of this thesis, we will consider fractures as a segment of a line, thus limit the network characterization to the geometrical and spatial domain. Therefore we will not cover the characterization of fracture's width, age, mineral fill or morphology.

4.1. Hough Characterization

The Hough transform combines in the same mathematical space the fracture geometrical and spatial attributes: the orientation, the trace length and the position. Thereby, the Hough diagram provides a visual overview of the geometry and the spatial distribution of the fractures. The orientation and distance to the origin (proxy for position) of a fracture can be read immediately from the location of its respective peak in the diagram, while its trace length can be inferred through its peak intensity. The spatial distribution of fractures can be observed on the diagram using, as proxy, the distribution of the peaks in the diagram. In particular, fracture clusters appear as peak clusters in the Hough accumulator. In this chapter, we refer to the cluster as a group of fractures closely spaced to each other, without necessarily intersecting.

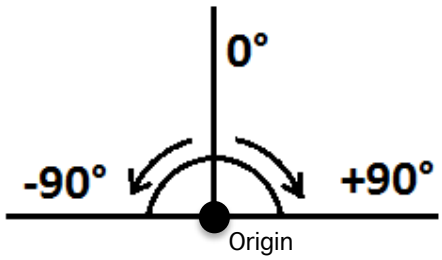

Figure 4.1: Convention used for determining fracture orientation

To understand how we can have an overview of a network geometry and spatial distribution, using the Hough transform, we propose to first study how different conceptual fracture networks are represented in the Hough space. Then, in the next section, we will apply this method on a real case study. There are multiple conventions to determine the orientation of a fracture. In the following we will use the orientation convention used in the MATLAB implementation of the Hough transform, as seen in figure 4.1, and arbitrarily position the origin at the top left corner of the image.

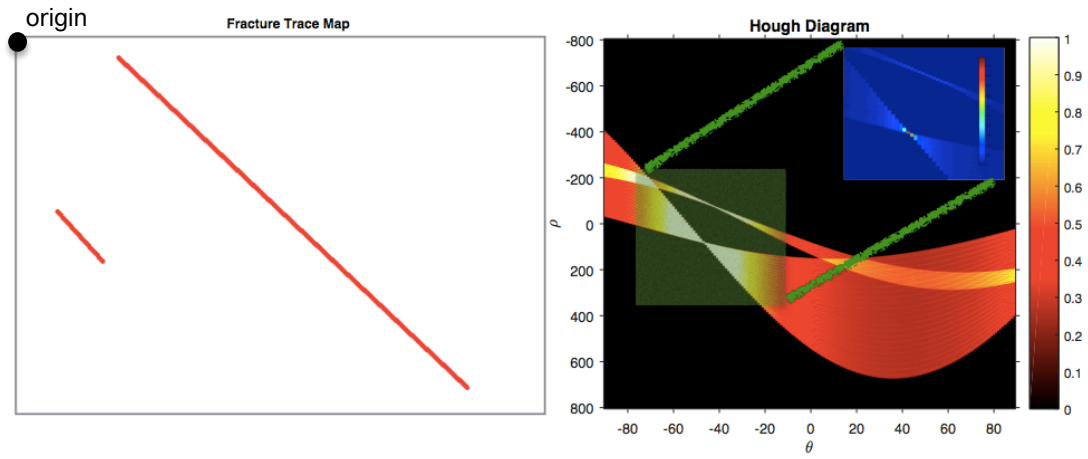

Figure 4.2: Case A

In case A, we have a network of two parallel lines with same orientation but with different lengths and axes. This corresponds, in the Hough diagram, to two colored traces, hereby called the spectrum, of different widths and with varying intensities. The peaks of intensity indicate the presence of lineaments. They are both located on the same orientation value (e.g. $\theta = -50°$), but at different distances from the origin (ρ).
The widest spectrum corresponds to the longest line. The wide span of the spectrum results from a larger amount of pixels "voting" in the accumulator. Moreover, peak intensities are also different. The longest line leads to a higher peak, as seen in the zoom of the Hough diagram, since there are more pixels to sum up in the accumulator array.

Nevertheless, computing the fracture length based on the peak intensity may not be straightforward. Indeed, if the trace is not a perfect lineament, the pixels belonging to the curvy part of the fracture will be erroneously accounted in the accumulator[1], and the peak intensity will be softened. In other words, the peak will not be as bright as it should be, which will lead to a underestimation of the fracture length. This effect is clearly observable in case D. Therefore, it is preferable, for trace length estimation, to limit the use of the Hough diagram to traces that are full lineaments.

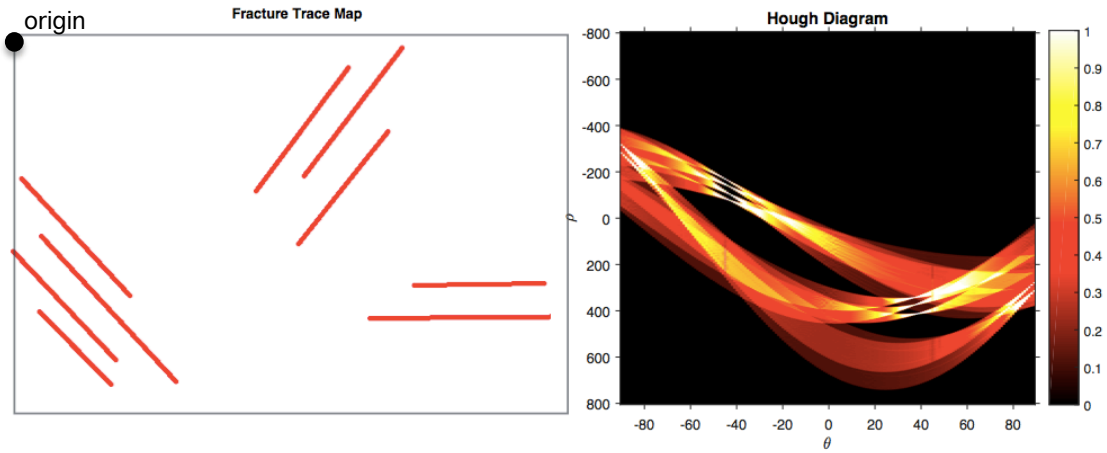

Figure 4.3: Case B

[1] As described in section 3.3.1

In case B, we have three clusters of orientations. This leads to three clusters of peaks, each located at their respective angle (i.e. $\theta = -40°; 90°; 40°$). The intensity of each peak and the span of each spectrum are similar since the length of the traces are similar.

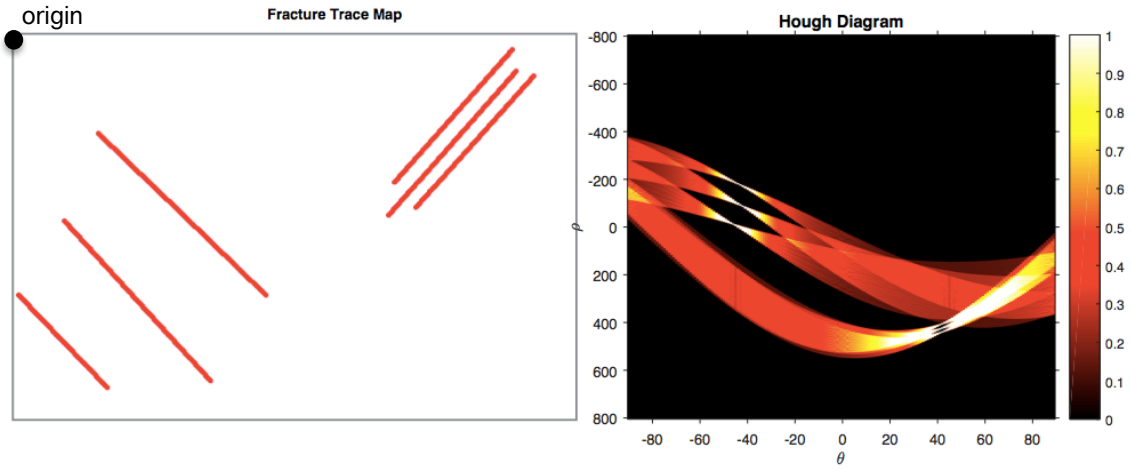

Figure 4.4: Case C

In case C, we have again two clusters of peaks in the Hough space. The cluster of fractures with an orientation of $+40°$ is denser, therefore it leads to a narrower spread of the peaks, which almost leads to a merging in one main peak[2]. Yet, this doesn't affect the peak's intensity, which remain similar for the six peaks.

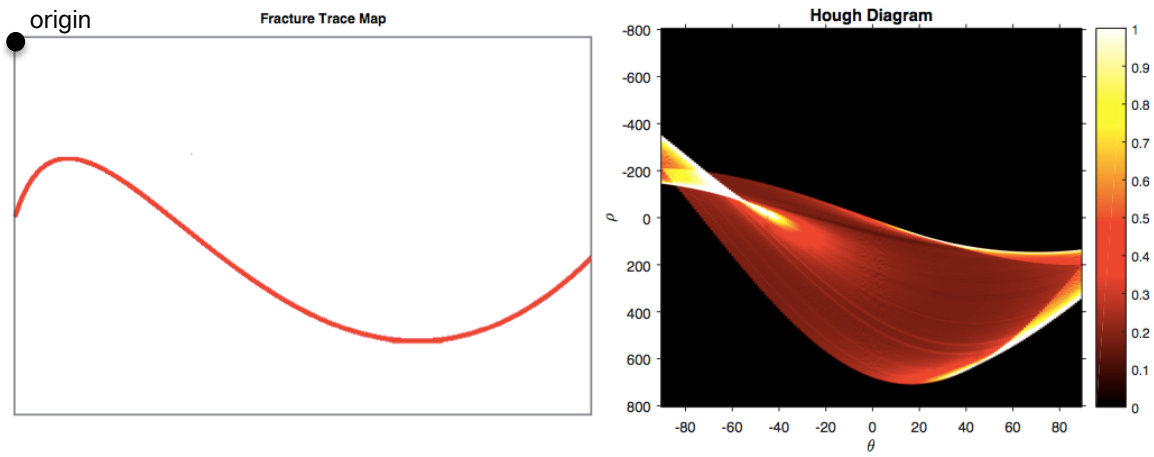

Figure 4.5: Case D

In case D, we have a feature which is curvy. We can still detect a peak in the Hough transform since there are still some lineaments in the curve, especially at $-60°$. Yet, the line trace is diluted in multiple small scale segments and we can hardly grasp the real nature of the curve, especially the peak's intensity which is far below the total fracture trace length. This is a perfect example of the dilution phenomenon described earlier. Therefore, applying the Hough transform to non-linear fracture networks

[2]It is interesting to note that as mentioned in section 3.2.2.5, a cancellation zone that is too large may lead to the detection of only one of the lines

is mostly irrelevant.

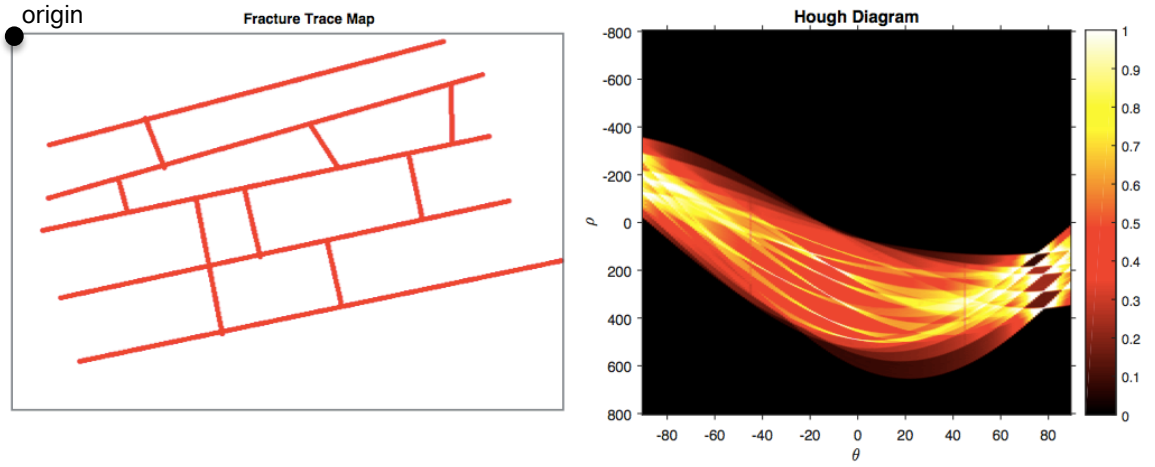

Figure 4.6: Case E

In case E, we deal with a much more realistic fracture network. In the Hough diagram we can observe a set of 5 peaks at $80°$. An another set of 8 lower intensity peaks are seen between $-40°$ and $-20°$. These peaks have a lower intensity, this can be seen with their dimmer and narrower spectrum, compared with the broads and brights spectrum around the 5 peaks. From these observations we can conclude that we have a network with a main trend of $80°$, with multiple smaller fractures oriented perpendicularly.

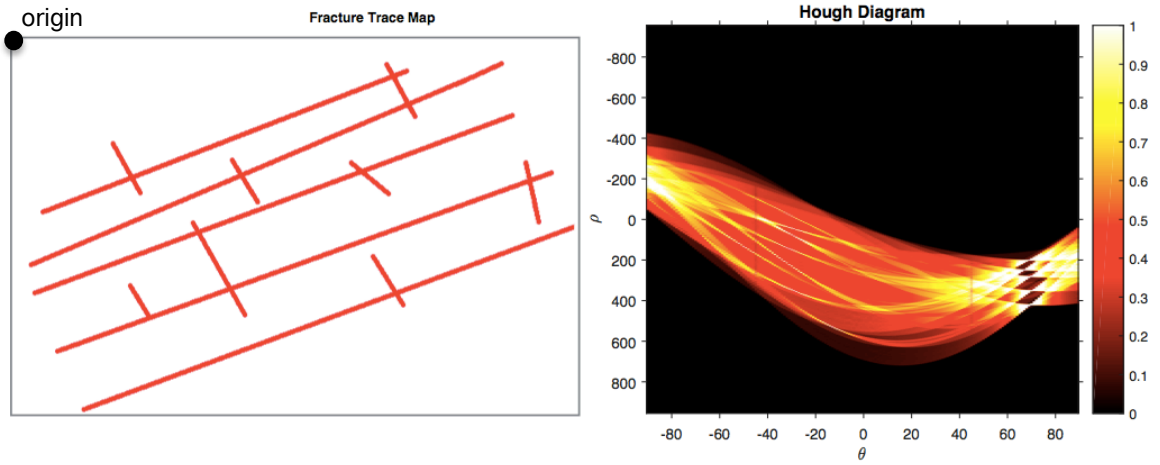

Figure 4.7: Case F

The network depicted in case F is similar to case E, except for the small perpendicular fractures which are shifted along their axis, changing their abutment with the main fractures. If, previously, we had fractures that were abutting with T connections, we now have, in this new case, mainly X and I connections. This new case highlights one of the main limitations of the Hough characterization: the Hough diagram is exactly the same as in E. Indeed the distance to the origin depicted by the parameter ρ defines the position of the axis of the fracture and not its actual position along this axis. Therefore the exact positioning cannot be described in the Hough space. This limits our appraisal of network topology and abutment characterization. However it is important to note that this limitation is valid only

if the fractures are shorter than the sample area. Indeed, if they are longer, the axis and the fracture are one, and this limitation become obsolete.

4.2. Case Study: Carbonates Outcrop in Potiguàr Basin

In this section we propose to characterize a fracture network based on the Hough transform to capture the network spatial distribution.
The data set used for this case study is a carbonate outcrop located in North East Brazil.

Figure 4.8: Outcrop AP3, used as experimental data set, and its manually tracked fracture network in red. *Source: van Eijk* (2014)

4.2.1. Geological Background

The outcrop belongs to the Cretaceous Jandaíra Formation which is a carbonate platform used as an analogue for the fractured reservoirs in the deep subsurface, offshore Brazil, which were deposited in the same facies setting as the Jandaíra formation [28].
The outcrop itself is 580 meters long and 300 wide. Dissolution occurred along fractures, faults and bedding planes, creating leaching pathways of increased secondary porosity and permeability [28].
At the surface, fractures, also known as barren fractures, have been enlarged by dissolution and weathering. Therefore, in an aerial view, fracture patterns can be clearly identified due to their shadows.

The data set has been acquired by *Bisdom* (2011) and interpreted by *van Eijk* (2014). The outcrop images have been acquired through UAV high definition imagery (i.e. resolution of 2cm/pixel). The

images were then exported as orthophotos into ArcGIS, where fractures were traced using tracer lines. The coordinates of the start and end points of each trace were listed in an attribute table in ArcGIS, as a DFN. The DFN properties are summarized in the following table:

Outcrop AP3: Summary	
Area	$120000m^2$
Number of Fractures	1396
Average Length	19.67m
Fracture Density	$0.0064[-/m^2]$

Table 4.1: Outcrop AP3 Summary *Source: van Eijk* (2014)

4.2.2. Hough diagram description

In this section we will analyze the Hough diagram of the fracture network, and see how it can provide us good indications of the fractures spatial distribution.

The outcrop image has been manually processed and interpreted by geologists to extract a discrete fracture network. The DFN is then transformed into a binary image where fracture traces are represented by a 1 while background is a 0. We then transform the binary image in the Hough space. To make it easier to see smaller peaks of intensity in the Hough diagram, we have chosen to use a surface plot to display the diagram. Peaks appear as maxima[3] in the plot.

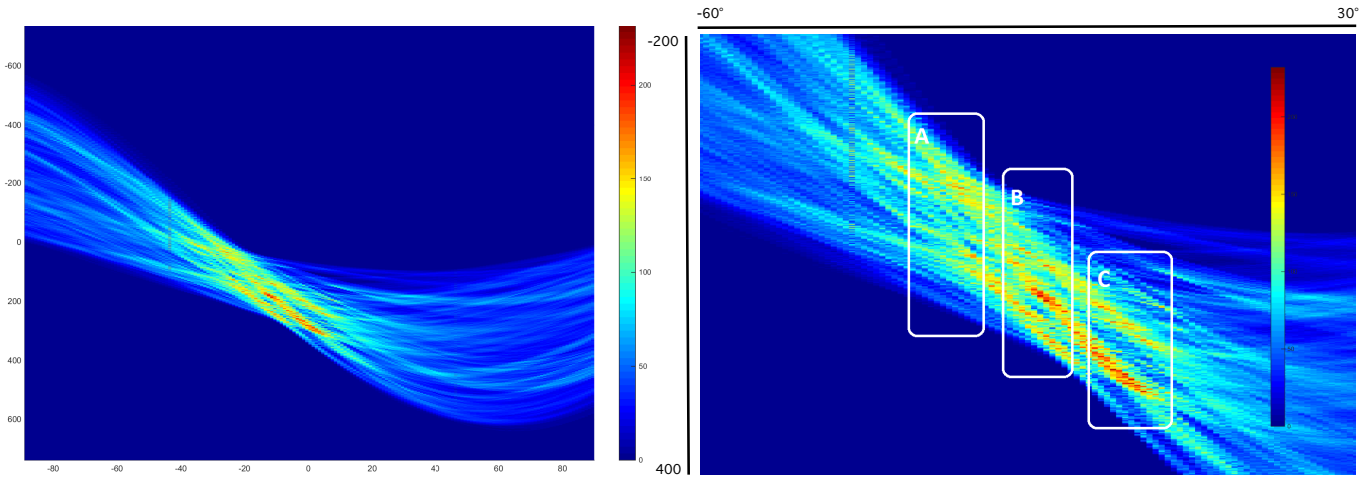

Figure 4.9: (a) Hough Diagram of the fracture network of AP3. (b) Zoom of the Hough diagram.

The first observation about the diagram in figure 4.9(a) is that the majority of the significant maxima appear in a orientation range comprised between -35° and 0°, forming a cluster of peaks. In this section we define cluster as a a group of closely spaced fractures, which do not necessarily intersect. Therefore a major proportion of the fractures will have an orientation falling within that range. This observation can be immediately confirmed when looking at the cross plot in figure 4.8, where we see that the main orientation trend is North-North-West.
We subdivide the cluster in three sections (box A B and C in figure 4.9)(b)), then show their respective fracture sets (of orientation corresponding to the range of the box), to investigate the information contained in the Hough diagram more closely.

First, around $-30°$ (box A: figure 4.10) we can observe in the Hough diagram a limited amount of isolated local maxima with a relatively low intensity. This would tend to show that in this orientation we have a limited amount of medium to short fractures, but spread across the outcrop with a relatively large spacing between each other. In figure (b) we see, as predicted, a couple of medium fractures

[3]To be consistent with our use of a surface plot, we will use the term maxima instead of peak

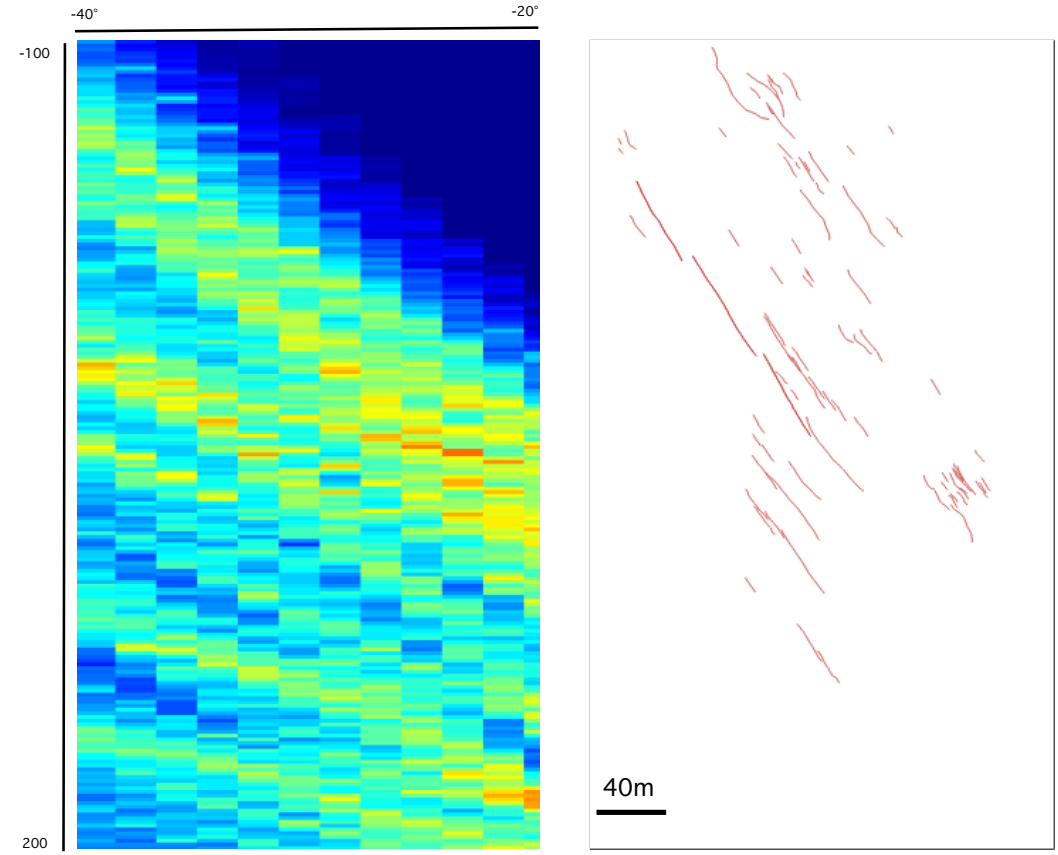

Figure 4.10: Hough Diagram zoomed on box A, with the corresponding fractures

accompanied with some smaller fractures evenly spread over the outcrop boundaries.

If we move toward orientations around $-10°$ (box B, figure 4.11), there are an increasing amount of local maxima; their intensity also tend to increase. This indicates that the fractures tend to be longer and more numerous. Moreover, we can see in the figure (a) that the maxima tend to concentrate in a sub cluster in the middle. This is an indication that we will observe a cluster of fractures of parallel orientation at this location.
Indeed, when looking figure (b) a clear cluster of fractures appears on the upper right side of the image. However, it is important to remember at this stage the limitation of the Hough transform when describing the position of fractures, presented in the previous section. The Hough transform describes the position of the axis of the fracture and not the fracture itself. Therefore it is possible that a bundle of coaxial fractures greatly spaced from each other appear as one cluster in the Hough diagram. Indeed, the small cluster located at the bottom of the outcrop on figure (b) will be, in the diagram, within the main cluster, since they share the same axis.

When shifting to orientations around $0°$ (box C, figure 4.12), a strong sub-cluster remains with high intensity peaks. Outside the clusters the maxima become less pronounced than in the previous box. Therefore, in the fracture trace map, we can still expect to find a cluster of parallel fractures with a few medium scale fractures located outside. In accordance with our prediction, we have less fractures and the expected cluster is observable on the lower right.

In conclusion, the AP3 case is a powerful proof of the potential of using Hough transform to capture the spatial distribution of a discrete fracture network. Indeed, a comprehensive overview of the network's spatial distribution has been obtained by some quick observations in the Hough Diagram. Orientation and distance to the origin have been predicted from each maxima location in Hough space, while length

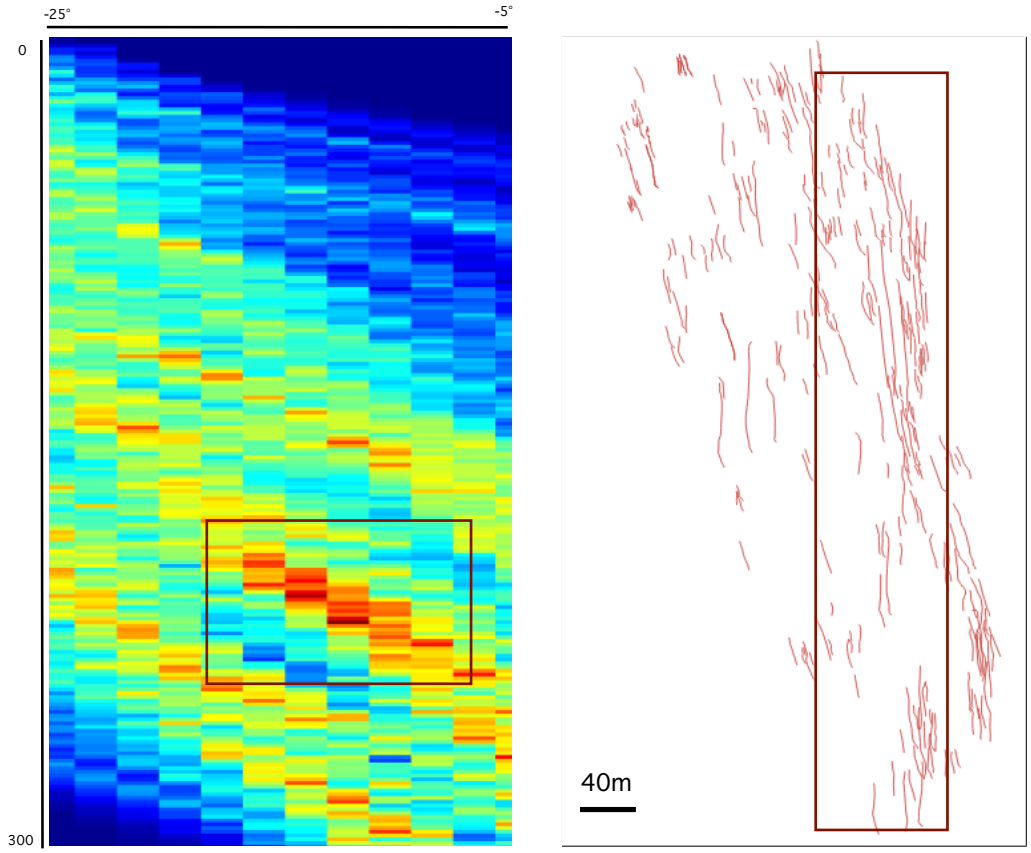

Figure 4.11: Hough Diagram zoomed on box B, with the corresponding fractures

of lineaments has been qualitatively inferred through maxima value.
The spatial distribution and clustering of fractures have been partially captured with the Hough diagram, since fractures that are closely spaced appear as closely spaced extrema in the Hough accumulator. Yet, we can only locate fracture axes and not their exact location.
Based on this potential, there is no doubt that introducing a more quantitative analysis of the Hough space could enhance our ability to grasp the spatial distribution of an arbitrary fracture network.
Nevertheless, this new domain representation can be used to reconstitute spatial distributions when creating stochastic discrete fracture networks. Indeed, if we honor the peak distribution in the Hough space, we will honor, in the same way, the spatial arrangement. In the following section we will study how the Hough Transform of a discrete fracture network can be used to drive a stochastic fracture network simulator.

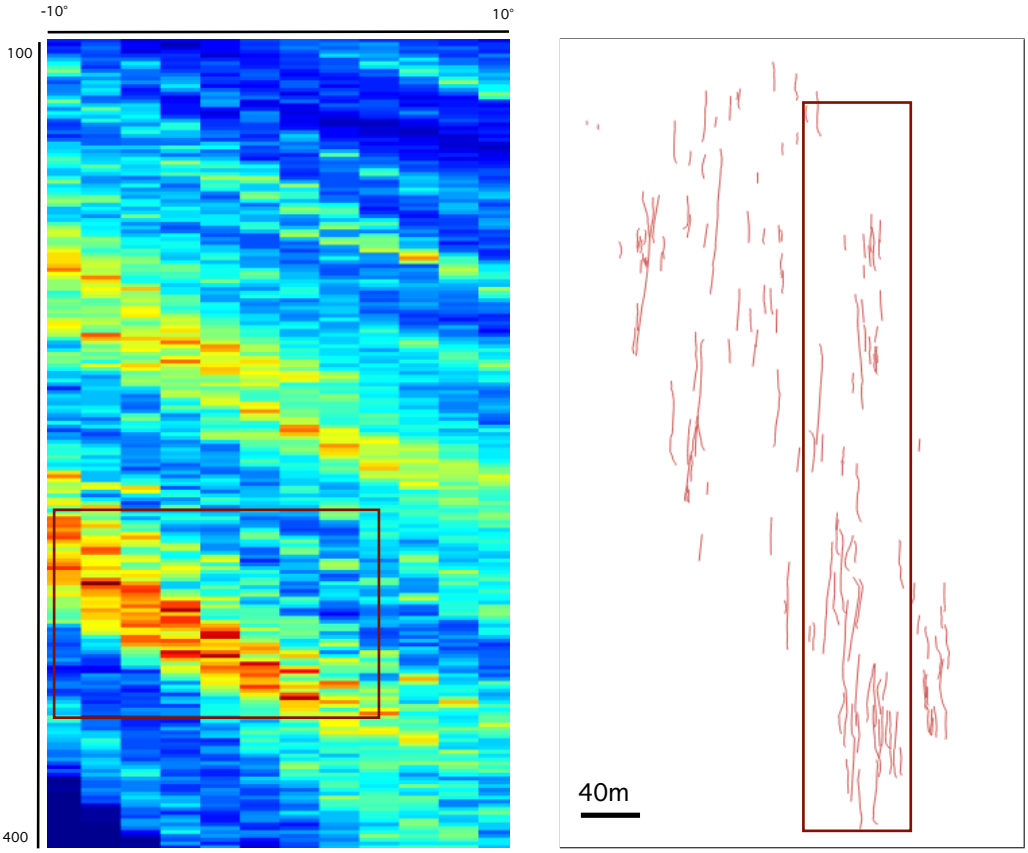

Figure 4.12: Hough Diagram zoomed on box C, with the corresponding fractures

5

Stochastic Discrete Fracture Network Simulation

In this chapter we present a stochastic discrete fracture network (DFN) simulator, fully implemented on MATLAB, based on the Hough parametrization.

We will show how the Hough parametrization has been used to drive our simulator to eventually create a DFN which conserves the geometrical attributes distribution and the spatial distribution of a fracture network observed in a outcrop (the source DFN). This will enable us to reproduce spatial trends observed in the field and integrate them in stochastic simulation to eventually increase the quality of the fracture network model.
By doing so, we create a third bridge in our work flow between image analysis and fracture simulation.

5.1. Methodology

Our program generates a fracture network based on a source discrete fracture network, in our case the outcrop AP3 introduced in the previous chapter.

The source DFN, as well as the generated network, are read and written in a database under the *.shp* format, which is a structure of N elements, where N is the number of fractures. Each element has 3 fields:

- **X:** X coordinates of the endpoints of the fracture
- **Y:** Y coordinates of the endpoints of the fracture
- **Bounding Box:** The coordinate of the smallest rectangle that contains the fracture.

From these data we can compute and create 3 additional fields used in the Hough parametrization: the length of the fracture (L), the orientation (θ) and the distance to the origin (ρ):

- $L = \sqrt[2]{(X(2) - X(1))^2 + (Y(2) - Y(1))^2}$
- $\theta = \arctan(\frac{X(2)-X(1)}{Y(2)-Y(1)})$
- $\rho = X(1) * cos(\theta) + Y(1) * sin(\theta)$

Our work flow will create fractures iteratively, one by one, as described in the figure 5.1 explaining our work flow.

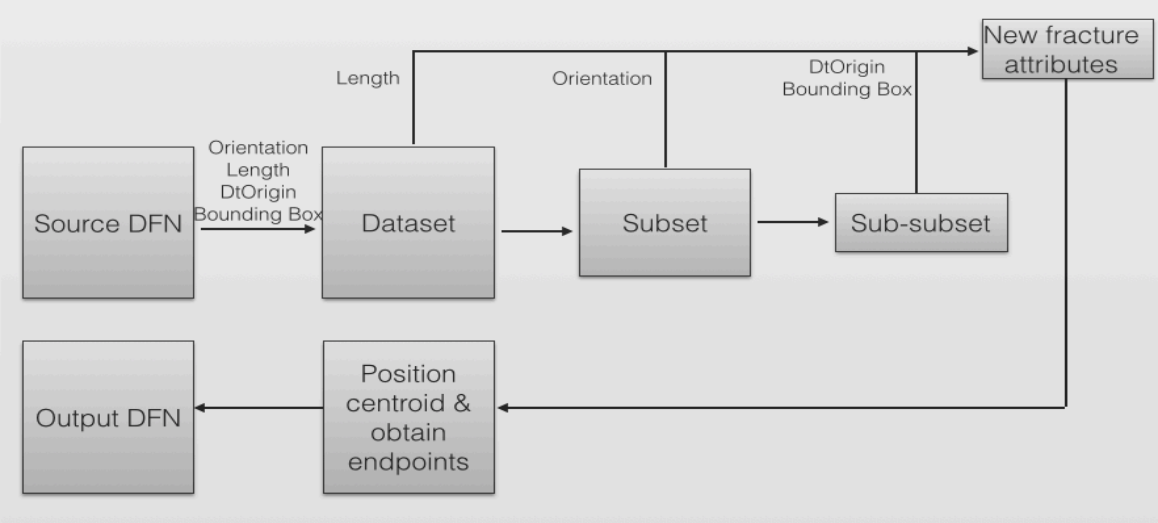

Figure 5.1: MATLAB Program's work flow

- **Step 1: Retrieve from source *.shp* the orientation, length and distance to the origin of every fractures and put each triplet in a database.**
- **Step 2: Sample a length from the database.**
- **Step 3: Create a subset of the database, containing fractures with a length difference below a certain threshold.**
  In our case we remove fractures with a length difference above 20% (arbitrarily).
- **Step 4: Sample an orientation (θ) from this subset.**
- **Step 5: Create a subset of the database, containing fractures with a orientation difference below a certain threshold.**
  In our case we remove fractures with an orientation difference above 20% (arbitrarily).
- **Step 6: Sample from this sub-subset a distance to the origin (ρ) and a bounding box belonging to the same fracture.**
- **Step 7: Put randomly the new fracture centroïd on the axis defined by <θ,ρ>, and within bounding box.**
- **Step 8: Calculate fracture end points.**
- **Step 9: Fill a new entry with the new fracture attributes in the output *.shp*.**
- **Step 10: Repeat from step 2 to generate a new fracture. Stop when N fractures have been generated.**

Figure 5.2: Description of each step

The fundamental principle of our methodology is to sample attributes from the database to create a new fracture. To do so, we use the *bootstrapping sampling*. This method draws values, with replacement, directly from the data set, without any assumptions as to what standard probability density function the

data set fits [5].

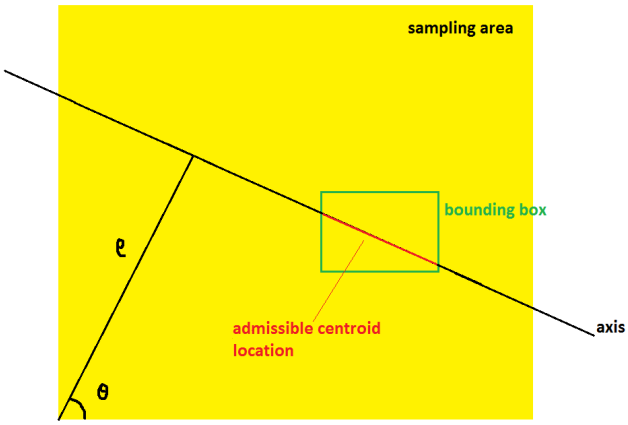

Figure 5.3: Centroid admissible position with sampled origin, distance to the origin and bounding box.

The reason to sample attributes from a subset at each step and not from the entire dataset is to preserve the correlation between the length (L), the orientation (θ) and the distance to the origin (ρ). Indeed, if we sample an orientation among a subset of fractures of similar length, we avoid drawing an orientation value that is not observed in the source DFN, for that given length.

The sampled orientation and distance to the origin allow us only to describe the axis to which the fracture belongs, but not the exact position of the fracture centroïd. This is the reason why we sample the bounding box at the same time as the distance to the origin. We then add a constraint on the centroïd location: being within the sampled bounding box (figure 5.3).

It is important to note that we didn't use the Hough transform directly in our stochastic DFN simulator. However, our work flow remains applicable to the Hough transform. Instead of sampling a length, an orientation and a distance to the origin from the *.shp* database, we can sample them from the Hough diagram. Indeed, we can sample a peak's intensity, a peak's orientation (θ) and a peak's distance to the origin (ρ) from the diagram as respective proxies for fracture length, orientation and distance to the origin.

5.2. Results

Based on the AP3 outcrops, we did 2 realizations (figure 5.4), that are similar in all aspects (fracture number, P20, length and orientation distribution, their correlation, as seen in table 5.1) except their spatial distribution. In the first realization, fractures are positioned based on the Hough parametrization (referred in the following as *Hough positioning*), while in the second model, fractures are positioned completely randomly inside the boundaries of the source DFN, using a *Poisson Point Process*.

Outcrop AP3: Summary	
Area	$120000m^2$
Number of Fractures	1396
Average Length	19.67m
P20	$0.0064[-/m^2]$

Table 5.1: Summary of the input used for the simulation; *Source: van Eijk* (2014)

We immediately observe that the Hough positioning reconstitutes the spatial structure of the primary network much more accurately. In order to quantify this observation we will compare the realizations based on clustering and geometrical properties.

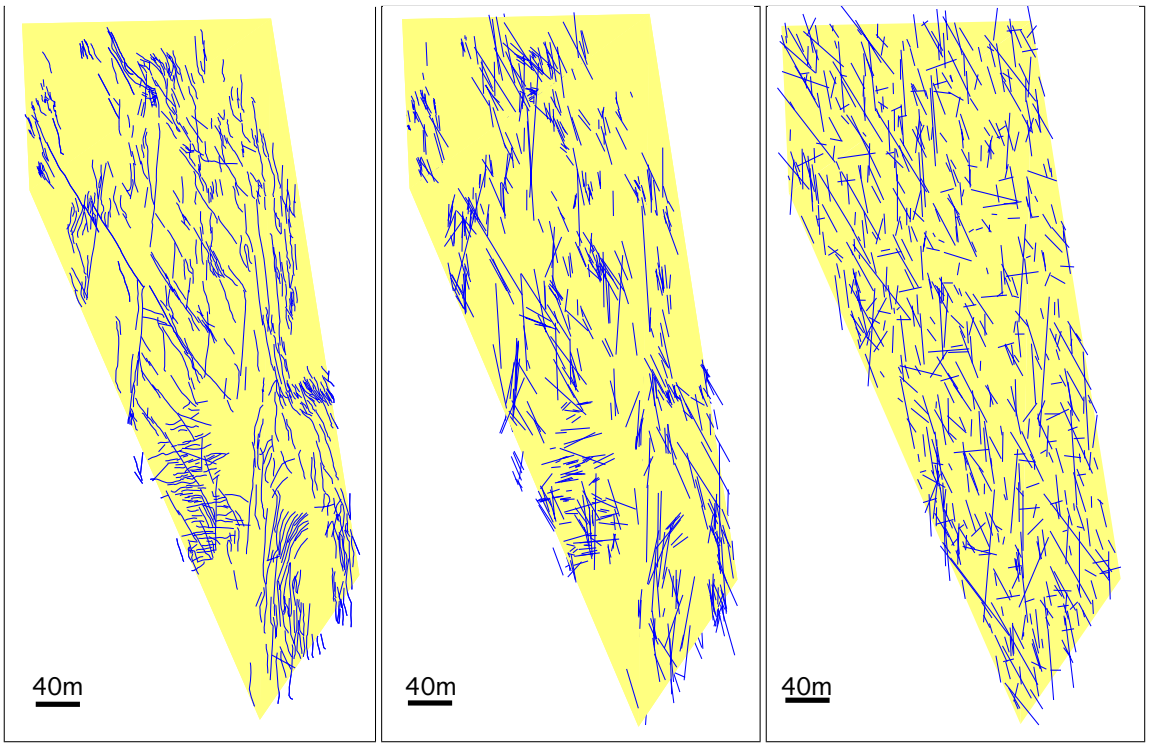

Figure 5.4: (a) The source DFN. (b) Stochastic realization with simulation driven by Hough transform. (c) Stochastic realization with fully random simulation. The yellow box represents the source DFN boundaries.

5.2.1. Geometrical Comparison

Due to our bootstrapping sampling method, we keep the initial distribution of geometrical attributes, no matter the positioning. This can be seen in figure 5.6, when we compare the length and orientation distributions. The similarity between those 3 distributions highlights the fact that the geometrical attributes' distributions are invariant no matter which positioning approach we've chosen.

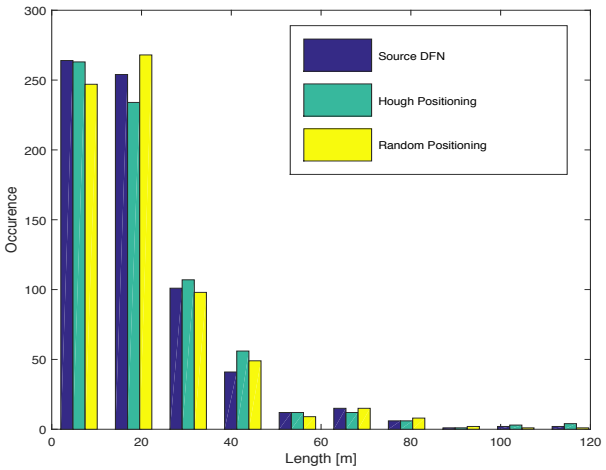

Figure 5.5: Length distribution different case: Source DFN (blue), Hough driven simulation (red) and fully random (green)

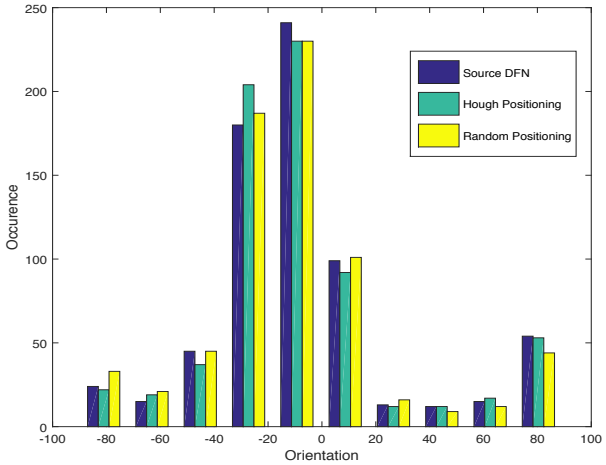

Figure 5.6: Orientation distribution different case: Source DFN (left), Hough driven simulation (middle) and fully random (right)

5.2.2. Clustering Comparison

We've highlighted in the literature review the importance of clustering (a set of fractures that are connected [2], where connectivity refers, in this thesis, to the instances where fractures intersect one another) for transport properties such as connectivity. We can first compare the amount of clusters: 80 clusters in the original DFN, 97 with a simulation using Hough and 281 with fully random positioning. This impacts the size of the different clusters when we compare their respective cumulative distributions [19], such as in figure 5.7. In this plot we see that the Hough positioning keeps the cluster size distribution almost unchanged, while the random positioning leads to significantly smaller clusters.

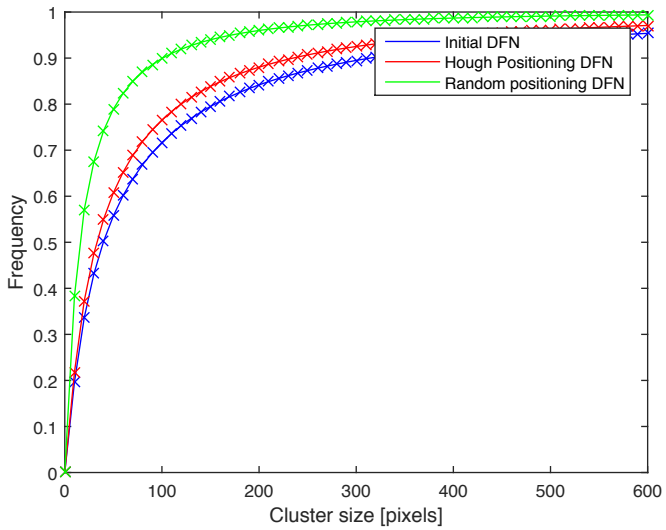

Figure 5.7: Comparison of the cluster size cumulative distribution between different realizations

Finally, we compare the size of the largest cluster for the three different cases, since it is the limiting factor in terms of network connectivity [19]. We have a cumulative trace length of 10.500 m in the largest cluster of the initial network, 6090 m for the Hough positioning and finally 980 m for the random realization (figure 5.8).

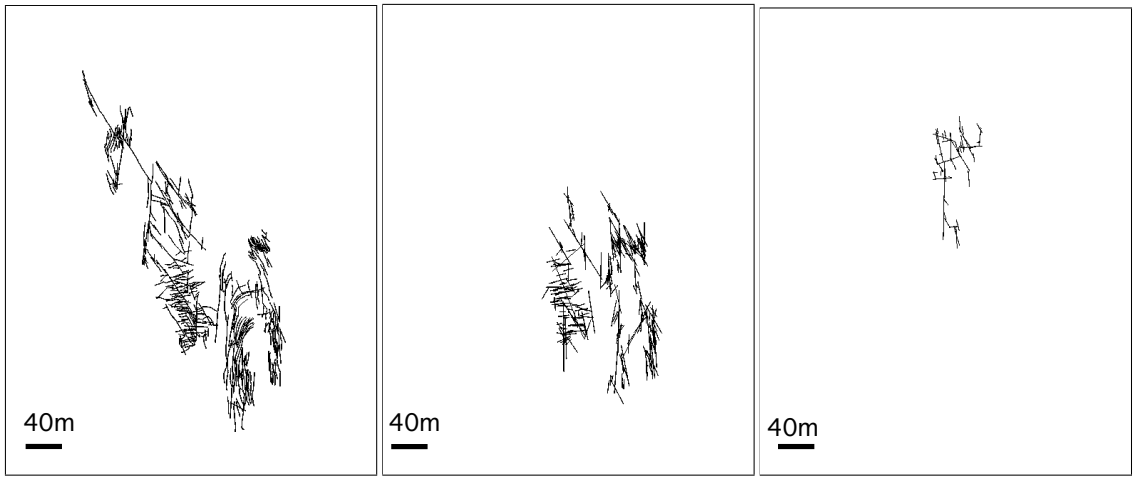

Figure 5.8: (a) Largest cluster in the source DFN. (b) Largest cluster, with simulation driven by Hough transform. (c) Largest cluster, with fully random simulation.

5.2.3. Well Connectivity Comparison

We can position an injector and a producer well (a doublet) at an arbitrary location, similar for both realization, and observe the maximum spacing at which the doublet remains connected (figure 5.9)[1].

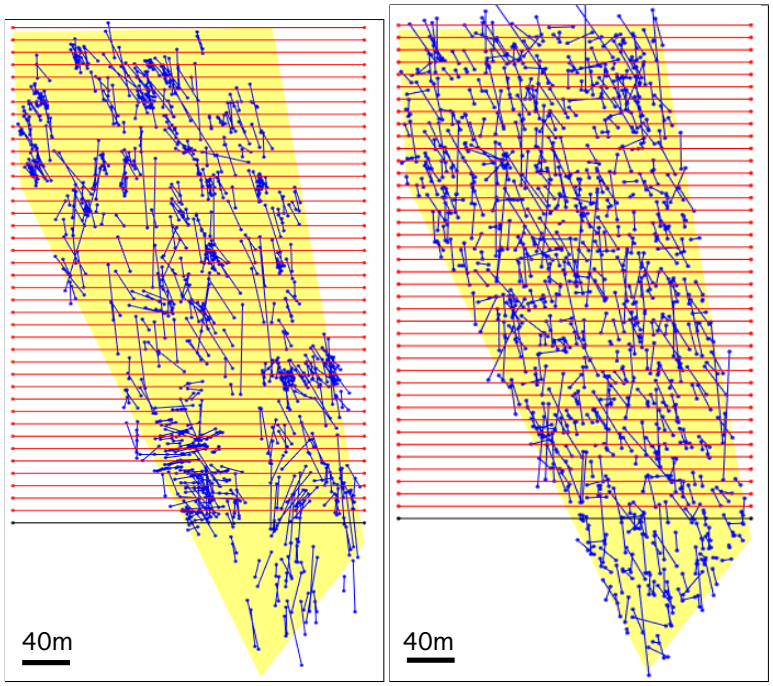

Figure 5.9: Position of the producing wells (red) and the injector (black), with one (arbitrary) network generated with our Hough based simulator (a) and for a simulator using random positioning (b).

In the source DFN the maximum spacing is 97 m, 104 m in the Hough based realization, and 60 m in the realization with random positioning.
In that sense, the well connectivity observed in the outcrop is better preserved in the Hough based

[1]The methodology to achieve this calculation is documented in Appendix A.

simulator than in the simulation positioning fractures randomly.

Indeed, we chose our well orientations to be perpendicular to the longest observed fractures in the source DFN, which are N-S trending. Therefore, these particular fractures will have a large influence in well connectivity since, if placed correctly, they will systematically intersect the injector and the producer. In the Hough driven simulation, these fractures will remain perpendicular to the pair of wells, since the length-orientation-position correlation is preserved. However, with the random positioning simulator, this specific spatial arrangement will not be represented: the orientation and position being randomly drawn, the longest traces may become rather parallel to the pair of wells, therefore underestimating the well connectivity.

5.2.4. Variability

Since our process is stochastic, we can expect variations between each DFN we generate each time. Quantifying this variability is important to appraise the consistency of our simulator.

First, we generate 3 DFNs with our Hough based simulator, and compare their cumulative cluster size distribution.

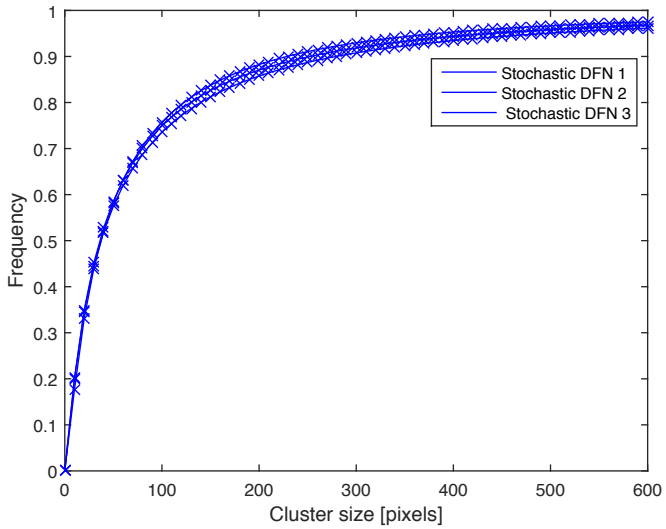

Figure 5.10: Comparison between cluster size cumulative distribution between realization

We observe in the figure 5.10, that the cluster size cumulative distribution does not vary significantly between each DFN. Therefore our simulator shows the same clustering trend for each realization.

In the same manner, the maximum spacing between a connected pair of wells is expected to vary among the different realizations. For that purpose, we generated 30 DFNs with both simulators (60 in total), and compared their doublet maximum spacing cumulative distributions (figure 6.1).

In this plot we see that the median of the maximum spacing for two connected wells is 105 m with the Hough based simulator, which is a deviation of 8 m with the doublet's maximum spacing observed in the outcrop. This deviation increases to 43m with the random positioning simulator (median at 140 m). There is also less variability in terms of maximum spacing with the Hough based simulator (steepest slope of the cumulative curve). Indeed, among the 30 DFNs made with random positioning, the observed doublet's maximum spacing varies between 40 m to 360 m, while it varies between 60 m and 220 m with the 30 DFNs made with the Hough based simulator.
This result was expected, because the Hough based simulator uses one more characterization pa-

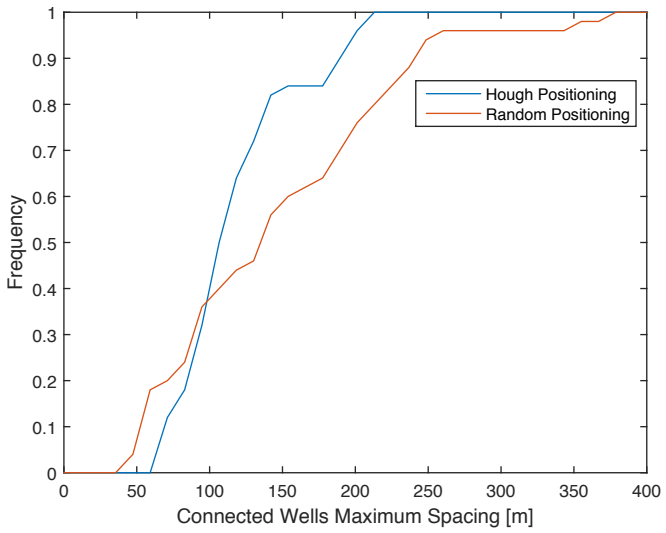

Figure 5.11: Connected wells' maximum spacing cumulative distribution for a simulator positioning fractures based on the Hough transform, and a simulator positioning fractures randomly.

rameter, the Hough transform, than a simulator using random positioning. Thus, in one sense, our simulator has less degrees of freedom, so the different realizations will tend to look more or less similar to each other.

5.3. Discussion

The results presented in the previous section highlight the potential of our simulation approach based on the Hough space. Our results did show that our approach recreates the spatial distribution of the fractures observed in outcrops with more accuracy (figure 5.4). This observation is confirmed when we compare the cluster size cumulative distribution (figure 5.7), the cluster maximal size (figure 5.8) or the wells' connectivity of our realizations (figure 6.1). In terms of geometry, the length and orientation distributions are conserved (figure 5.6).
The variability analysis shows that the modeled DFNs are consistent in the sense that they share the same clustering and well connectivity trends.

Another major improvement of our method is the use of the Hough transform as input for our simulation. This eventually enables us to run a stochastic DFN simulator based on the Hough transform of an aerial image of an outcrop, avoiding the time consuming step of the manual interpretation and digitization of the outcrop image.

This innovative approach needs to be put in perspective of the intrinsic issues of the quantitative Hough space analysis discussed in the chapter 4. In particular, curvy fractures cannot be properly seen in the Hough space, or at least their length cannot be properly estimated. Also, we cannot determine if a peak in the Hough diagram corresponds to a single trace, or to multiple coaxial traces. Therefore, the sampling of fracture attributes from the Hough diagram remain difficult. Overcoming this issue would enable us to accurately use the Hough diagram as input for our stochastic simulation and greatly enhance our simulation capabilities.

Beyond the intrinsic issue of the Hough transform, we can also point out the difficulty of upscaling our model.
It is due to truncation bias: the fractures present in the outcrop are not exhaustive of all the fractures potentially present in the subsurface. For example, if our outcrop domain is 100x100m, we will be

unable to observe fractures longer than 100m. The corollary being that we will not sample fractures longer than 100m in our stochastic DFN.
It is also because the Hough transform is defined within a finite range of distance to the origin (ρ) corresponding to the largest ρ observed in the outcrop. Thus, if we want to generate a larger model (e.g. at reservoir scale), sampling a distance to the origin beyond the Hough diagram range will not be possible. The corollary being that positioning fractures, based on the Hough diagram, outside the outcrop boundaries is currently not possible.

In conclusion, the method is, in its current form, already a valuable enhancement compared to other stochastic methods.
Indeed, our work flow highlights the possibility to run fracture networks simulation based on the Hough transform of outcrop aerial images. Furthermore, our method significantly contributes to the enhancement of the reproduction of spatial trends, such as clustering and well connectivity, observed in the field, making stochastic networks closer to what is observed in the nature.

6

Conclusion

In this project we've developed a comprehensive work flow that intended to bridge a gap between the fields of remote sensing and geology, in particular fracture network characterization and stochastic network generation.

In the first phase of this project we've focused on image analysis techniques that could automate fracture detection. If our results highlight the difficulty of addressing this specific task, mainly due to the complexity of aerial images, we introduce an interesting way to characterize the image: the Hough transform method. If this method shows some limitations to accurately extract the fracture pattern, it offers a new way to capture the spatial arrangement of the fracture network.

We've showed in the fourth chapter how this description was innovative, particularly because it integrates fracture length, orientation and spatial distribution in the same space enabling us to make cross correlations. With a couple of conceptual examples, and then a case study in Brazil, we've highlighted the power and the potential of the Hough characterization. Unfortunately, this method has limitations, and, if a qualitative description of the spatial arrangement is possible, the road to obtaining an accurate quantitative characterization is still long.

Nevertheless, in the fifth chapter, we saw how the Hough transform offers an innovative way to enhance the fracture's spatial distribution in stochastic discrete fracture network simulation, making DFNs closer to what is observed in the field, in terms of clustering or wells' connectivity. But, we also highlighted the difficulty to accurately sample fractures attributes in the Hough diagram and showed the difficulty of upscaling our model to an area larger than the domain of the outcrop. In particular, the Hough diagram is not defined beyond the outcrop domain, thenceforth we can not use the Hough transform to position the fractures outside the outcrop boundaries. Solving these issues would greatly improve our DFN simulation capabilities.

In conclusion, what is new in this thesis is the idea to use to the Hough space to characterize a fracture network. This approach offers us a way to characterize the network directly from an aerial image or a fracture trace map. This characterization offers an innovative approach to extract fracture patterns from aerial images, but also enhances our stochastic network simulation capabilities. Indeed the use of Hough based positioning makes stochastic fracture networks more natural in the sense they can describe phenomenon observed in outcrop such as clustering correlation.

This work should be an incentive to endeavor to integrate more research between image analysis, remote sensing, geology and reservoir engineering. Indeed we have shown the potential of the application of image analysis tools to a geological issue: the characterization of fracture networks.

Acknowledgment

I would like to thanks my supervisors, Giovanni Bertotti, Nico Hardebol, Kevin Bisdom and Beril Sirmacek, for their continuous and thorough guidance, comments, reviews and support.

I thanks everyone who helped me, in a direct or indirect way, to complete my thesis, and in particular Barnes and Chris.

This being the last line I've wrote in my thesis, and thus in my entire university education, I would like to emphasize my gratitude to my supporters during these 6 long years: my parents. Without them, nothing would have been possible; they deserve all the credits for what have been achieved during these 6 years.

Figure 6.1: I would also like to thanks the oil prices ($/barrel).

Appendices

A

Wells' Connectivity Methodology

The probability that a pair of wells separated by a distance s is connected in a network generated by a stochastic simulation is designed by $p_h(s)$, if the simulator is based on the Hough transform, and $p_r(s)$ if the simulator position fractures randomly. To compute these functions, we will create a number of DFNs: N_h with our Hough based simulator, and N_r with a simulator which positions fractures randomly, all DFNs are reconstructed based on the same source DFN.
For a pair of wells separated by a distance $\bar{s}$ (figure A.1), identically positionned in every DFNs, we will observe $N_h(\bar{s})$ connected doublet in the first set and $N_r(\bar{s})$ in the second. Therefore, to estimate the probability that the two wells are connected, we will use the following estimator:

$$\hat{p}_i(s) = \frac{N_i(s)}{N_i}$$

Where i can either be h or r, depending the simulator we are considering.

To determine if the pair of wells in a given DFN is connected or not, we use the *Dijkstra* Algorithm. This algorithm, inherited from Graph Theory, determines if two set of fractures are connected by at least one path [4].
The first step of the algorithm is to create 2 sets of fractures: one made of fractures intercepting the producer well, while the second is made of fractures intercepting the injector well.
Then, for a fracture network made of M fractures, we label each fracture with a unique number comprised between 1 and M.
Subsequently, we create a MxM matrix define as follow:

$$\begin{pmatrix} \delta_{1,1} & \cdots & \delta_{1,M} \\ \vdots & \ddots & \vdots \\ \delta_{M,1} & \cdots & \delta_{M,M} \end{pmatrix} \quad \text{where} \quad \left\{ \begin{array}{c} \delta_{i,j} = 1, \text{ if fracture } i \text{ intersect fracture } j \\ \delta_{i,j} = 0, \text{ otherwise} \end{array} \right\}$$

The MATLAB implementation of the *Dijkstra* algorithm use this matrix as an input to determine if the two sets of fractures are connected by, at least, one path. If a path exists, the wells are connected.

We summarize the work flow to construct the probability function in the following scheme.

- **Step 1: Create N_h DFNs with our Hough based simulator and N_r with the fully random simulator.**
  In our case $N_h = N_r = 30$.
- **Step 2: Set the location of the injector well identically in every DFNs.**
  In our case, with an orientation West-East (see figure A.1).
- **Step 3: Pick a well spacing value $\bar{s}$, and position the producer well identically in every DFNs, parallel to the injector.**

- **Step 4: Use Dijkstra Algorithm on every DFNs and calculate the amount of connected doublet $N_h(\bar{s})$ and $N_r(\bar{s})$**
- **Step 5: Calculate doublet connectivity probability $\hat{p}$ for the spacing $\bar{s}$**
- **Step 6: Repeat from step 3 with a different spacing value**

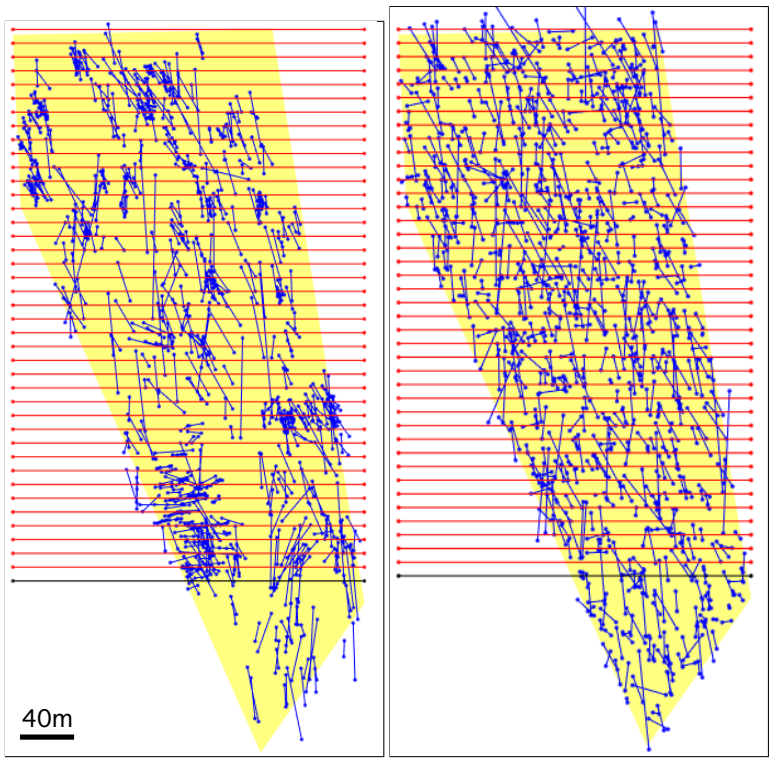

Figure A.1: Position of the producing wells (red) and the injector (black), with one (arbitrary) network generated with our Hough based simulator (a) and for a simulator using random positioning (b).

Bibliography

[1] Kevin Bisdom. Modelling 3d discrete fracture networks using 2d outcrop data. *TU Delft, Master Thesis in Applied Earth Sciences*, 2011.

[2] Olivier Bour. Transferts des fluides en milieux poruex, effets d'echelle. [fluid transfer in porous media, scaling effect]. *Université de Rennes, PhD Thesis*, 1996.

[3] B. Bourbiaux, R. Basquet, MC. Cacas, and JM. Daniel. An integrated workflow to account for multi-scale fractures in reservoir simulation models: Implementation and benefits. *SPE 78489*, 2002.

[4] JC. Delvenne. Théorie et algorithmique des graphes: Notes de cours [graph theory and algorithm: syllabus]. *Applied Mathematics dept., Catholic University of Louvain (Belgium)*, 2014.

[5] P. Diaconis and B. Efron. Computer-intensive methods in statistics. *Scientific American*, pages 116–130, 1983.

[6] Richard O. Dud and Peter E. Hart. Use of the hough transformation to detect lines and curves in pictures. *Communication of the ACM*, 15:11–15, 1972.

[7] Tom Bratton et Al. The nature of naturally fractured reservoirs. *Schlumberger Oilfields Review*, pages 1–23, 2006.

[8] A. M. Ferrero, G. Forlani, R. Roncella, and H. I. Voyat. Advanced geostructural survey methods applied to rock mass characterization. *Rock Mech Rock Eng*, 42:631–665, 2009.

[9] Rafael C. Gonzalez and Richard E. Woods. Digital image processing. *Prentice Hall*, page 316, 2008.

[10] Steve Harwin and Arko Lucieer. Assessing the accuracy of georeferenced point clouds produced via multi-view stereopsis from unmanned aerial vehicle (uav) imagery. *Remote Sensing*, 4:1573–1599, 2012.

[11] John A. Howell, Allard W. Martinius, and Timothy R. Good. The application of outcrop analogues in geological modeling: a review, present status and future outlook. *The Geological Society, Special Publications*, 387:1–25, 2014.

[12] John Hudson. Rock characterization. *ISRM Symposium: Eurock*, 1992.

[13] L. Jing. A review of techniques, advances and outstanding issues in numerical modelling for rock mechanics and rock engineering. *Journal of Rock Mechanics and Mining Sciences*, 40:283–353, 2003.

[14] Arnon Karnieli, Amnon Meisels, Leonid Fisher, and Yaacov Arkin. Automatic extraction and evaluation of geological linear features from digital remote sensing data using a hough transform. *Photogrammetric Engineering and Remote Sensing,*, 62:525–531, 1996. doi: 0099-1112/96/6205-5.

[15] J. Long and D. Billiaux. From field data to fractures modeling: an example using spatial structure. *Water Resources Res.*, 23:1201–1216, 1987.

[16] Schlumberger Ltd. Characterization of fractured reservoir. predictive models to optimize carbonate reservoir performance. *Schlumberger Information Brochure*, 2008.

[17] S. Mahendran. A comparative study on edge detection algorithms for computer aided fracture detection systems. *International Journal of Engineering and Innovative Technology*, 2, 2012.

[18] MATLAB. *Hough function documentation. version 7.10.0 (R2015a)*. The MathWorks Inc., Natick, Massachusetts, 2015.

[19] Noelle E. Odling. Network properties of a two-dimensional natural fracture pattern. *Journal of Natural Gas Science and Engineering*, 138:95–114, 1992.

[20] Mohsen Nazari Ostad, Omid Asghari, Xavier Emery, Mehran Azizzadeh, and Farhad Khoshbakht. Fracture network modeling using petrophysical data, an approach based on geostatistical concepts. *Journal of Natural Gas Science and Engineering*, 31:758–768, 2016.

[21] Axelle Pochet, Francois Bonneau, Guillaume Caumon, and Judith Sausse. Discrete fracture network generation from induced microseismicity data: a method based on 3d hough transform. *33rd GOCAD-MEETING*, 2013.

[22] David J. Sanderson and Casey W. Nixon. The use of topology in fracture network characterization. *Journal of Structural Geology*, 72:55–66, 2015.

[23] Augusto Sarti and Stefano Tubaro. Detection and characterisation of planar fractures using a 3d hough transform. *Signal Processing*, 82:1269 – 1282, 2002.

[24] Beril Sirmaçek and Cem Ünsalan. Road detection from remotely sensed images using color features. *German Aerospace Center (DLR), Remote Sensing Technology Institute*, ASK COMPLETE REF.

[25] D. Stoyan and H. Stoyan. Fractal, random shapes and point fields. *John Wiley and sons*, 1994.

[26] John B. Thurmond, Tore M. Løseth1, Jan C. Rivenæs, Ole J. Martinsen, Carlos Aiken, and Xueming Xu. Using outcrop data in the 21st century – new methods and applications, with example from the ainsa turbidite system, ainsa, spain. *University of Texas in Dallas, Center for Lithospheric Studies*, 2005.

[27] D. Turner, A. Lucieer, and C. Watson. An automated technique for generating georectified mosaics from ultra-high resolution unmanned aerial vehicle imagery, based on structure from motion point clouds. *Remote Sensing*, 4:1392–1410, 2012.

[28] Mariska M. van Eijk. Analysis of the fracture network in carbonate rocks of the jandaíra formation in northeast brazil. *TU Delft, Master Thesis in Applied Earth Sciences*, 2014.

[29] Yathunanthan Vasuki, Eun-Jung Holden, Peter Kovesi, and Steven Micklethwaite. Semi-automatic mapping of geological structures using uav-based photogrammetric data: An image analysis approach. *Computers and Geosciences*, 69:22–32, 2014.

[30] Conny Zeeb, Enrique Gomez-Rivas, Paul D. Bons, and Philipp Blum. Evaluation of sampling methods for fracture network characterization using outcrops. *AAPG Bulletin*, 97, 2013.

[31] Yongjun Zhang, Lijuan Hao, and Jinxin Xiong. Photogrammetric processing of low-altitude images acquired by unpiloted aerial vehicles. *The Photogrammetric Record*, 26:190–211, 2011.